Article

Immunity

Quantitative control of *Ets1* dosage by a multi-enhancer hub promotes Th1 cell differentiation and protects from allergic inflammation

Graphical abstract

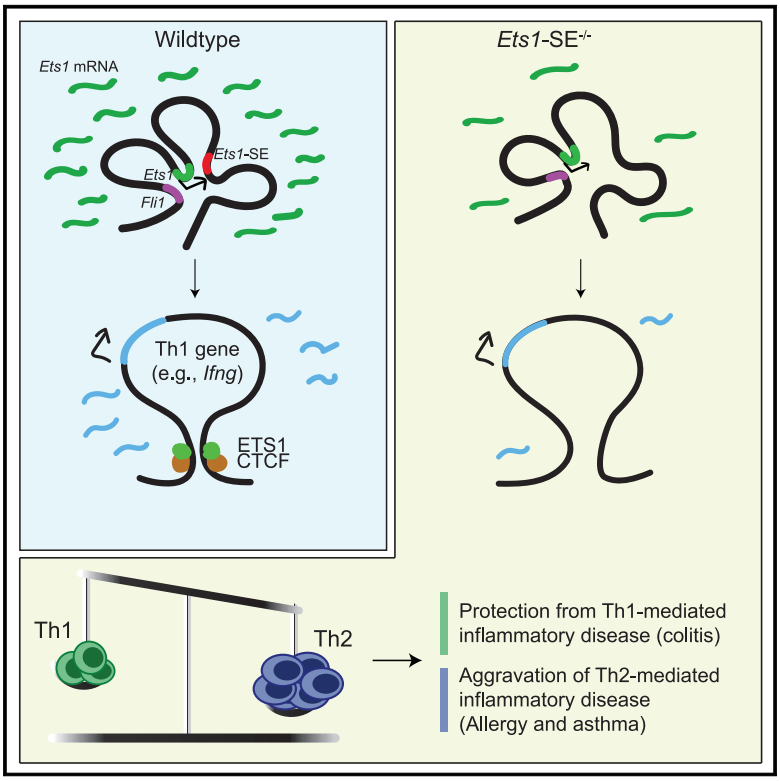

Highlights

- *Ets1* locus forms a multi-enhancer hub containing a super-enhancer called *Ets1*-SE
- *Ets1*-SE is required for Th1 differentiation and the *Ets1* gene dosage control
- Deletion of *Ets1*-SE leads to protection against colitis and an overt allergic response
- *Ets1* dosage controls the Th1-specific genome topology through the recruitment of CTCF

Authors

Aditi Chandra, Sora Yoon, Michaël F. Michieletto, ..., Barbara L. Kee, Jorge Henao-Mejia, Golnaz Vahedi

Correspondence

jhena@pennmedicine.upenn.edu (J.H.-M.), vahedi@pennmedicine.upenn.edu (G.V.)

In brief

Multi-enhancer hubs are spatial clusters of enhancers present across numerous developmental programs. Chandra, Yoon, Michieletto, et al. examine the functional relevance of multi-enhancer hubs in T cell biology and show that the multiplicity of enhancers interacting with the *Ets1* gene is essential to control the precise dosage of *Ets1* in response to cytokine cues, and the failure to do so can lead to allergic diseases.

Chandra et al., 2023, Immunity *56*, 1–17
July 11, 2023
https://doi.org/10.1016/j.immuni.2023.05.004

CellPress

Immunity

CellPress

Article

Quantitative control of *Ets1* dosage by a multi-enhancer hub promotes Th1 cell differentiation and protects from allergic inflammation

Aditi Chandra,[1,2,3,4,5,10] Sora Yoon,[1,2,3,4,5,10] Michaël F. Michieletto,[6,7,10] Naomi Goldman,[1,2,3,4,5] Emily K. Ferrari,[1,2,3,4,5] Maryam Abedi,[1,2,3,4,5] Isabelle Johnson,[1,2,3,4,5] Maria Fasolino,[1,2,3,4,5] Kenneth Pham,[8] Leonel Joannas,[2,6,7] Barbara L. Kee,[9] Jorge Henao-Mejia,[2,4,5,6,7,*] and Golnaz Vahedi[1,2,3,4,5,11,*]

[1]Department of Genetics, Perelman School of Medicine, University of Pennsylvania, Philadelphia, PA 19104, USA
[2]Institute for Immunology, Perelman School of Medicine, University of Pennsylvania, Philadelphia, PA 19104, USA
[3]Epigenetics Institute, Perelman School of Medicine, University of Pennsylvania, Philadelphia, PA 19104, USA
[4]Institute for Diabetes, Obesity and Metabolism, Perelman School of Medicine, University of Pennsylvania, Philadelphia, PA 19104, USA
[5]Abramson Family Cancer Research Institute, Perelman School of Medicine, University of Pennsylvania, Philadelphia, PA 19104, USA
[6]Department of Pathology and Laboratory Medicine, Perelman School of Medicine, University of Pennsylvania, Philadelphia, PA 19104, USA
[7]Division of Protective Immunity, Department of Pathology and Laboratory Medicine, Children's Hospital of Philadelphia, University of Pennsylvania, Philadelphia, PA 19104, USA
[8]Perelman School of Medicine, University of Pennsylvania, Philadelphia, PA 19104, USA
[9]Department of Pathology, Committees on Cancer Biology and Immunology, University of Chicago, Chicago, IL 60637, USA
[10]These authors contributed equally
[11]Lead contact
*Correspondence: jhena@pennmedicine.upenn.edu (J.H.-M.), vahedi@pennmedicine.upenn.edu (G.V.)
https://doi.org/10.1016/j.immuni.2023.05.004

SUMMARY

Multi-enhancer hubs are spatial clusters of enhancers present across numerous developmental programs. Here, we studied the functional relevance of these three-dimensional structures in T cell biology. Mathematical modeling identified a highly connected multi-enhancer hub at the *Ets1* locus, comprising a noncoding regulatory element that was a hotspot for sequence variation associated with allergic disease in humans. Deletion of this regulatory element in mice revealed that the multi-enhancer connectivity was dispensable for T cell development but required for $CD4^+$ T helper 1 (Th1) differentiation. These mice were protected from Th1-mediated colitis but exhibited overt allergic responses. Mechanistically, the multi-enhancer hub controlled the dosage of *Ets1* that was required for CTCF recruitment and assembly of Th1-specific genome topology. Our findings establish a paradigm wherein multi-enhancer hubs control cellular competence to respond to an inductive cue through quantitative control of gene dosage and provide insight into how sequence variation within noncoding elements at the *Ets1* locus predisposes individuals to allergic responses.

INTRODUCTION

The induction of immune responses is based on the modification of a common theme, where the cells responsible for detecting pathogens release one set of cytokines to stimulate lymphocytes and produce a second set of cytokines which in turn, trigger effector responses.[1] This multi-tiered response is largely instructed by transcription factor networks which transmit extrinsic signals to the nucleus and orchestrate transcriptional responses largely by acting on noncoding regulatory elements called enhancers. Transcription factors can exert their effect by establishing chromatin accessibility,[2–4] histone acetylation,[5,6] or DNA demethylation[7] at enhancer sequences. Consistent with the notion that enhancer function requires physical proximity with promoters of target genes,[8] the contributions of transcription factors on genome organization and enhancer-promoter interactions have been reported.[9–12]

Recent advances in genomics and imaging technologies attest to the formation of spatial clusters of enhancers, called interchangeably as multi-enhancer hubs,[13–20] 3D cliques,[21,22] *cis*-regulatory domains,[23] interacting triplets,[24] connected gene communities,[25] or architectural stripes.[26,27] Multi-enhancer connectivity at cell-fate determining genes play key roles in pluripotent stem cells,[28] immune cells,[22,29] as well as neurons.[30] Modulation of signal-dependent transcription factors such as Notch[21] and AP-1 family proteins[13,31] can alter connectivity within multi-enhancer hubs. Despite these examples, the functional and mechanistic link between multi-enhancer hubs, transcription factor networks, and immune responses is not well understood.

Please cite this article in press as: Chandra et al., Quantitative control of *Ets1* dosage by a multi-enhancer hub promotes Th1 cell differentiation and protects from allergic inflammation, Immunity (2023), https://doi.org/10.1016/j.immuni.2023.05.004

Here, we mathematically defined the higher-order structure of multi-enhancer interactions in mouse thymocytes.[22] One of the most hyperconnected regions in T cells occurred at a locus harboring E26 transformation-specific (ETS) 1 (*Ets1*) and Friend leukemia integration 1 (*Fli1*) genes. Although numerous single-nucleotide polymorphisms (SNPs) associated with immune-mediated diseases were distributed across the human ETS1-FLI1 locus, a noncoding region within this locus formed a hotspot for SNPs associated with type 2 immune diseases including allergy, asthma, and atopic dermatitis.[32,33] Deletion of the regulatory element in the *Ets1* locus associated with type 2 immune diseases in mice did not affect T cell development but impaired $CD4^+$ T helper 1 (Th1) cell differentiation, leading to protection against colitis and an overt allergic response. Mechanistically, the multiplicity of enhancer interactions at the *Ets1* locus controlled the sharp increase in the expression of *Ets1* in response to changes in the cytokine environment which in turn was required for the recruitment of CTCF to specify enhancer-promoter long-range interactions in Th1 cells. Considering that Th1 differentiation is a critical mechanism by which type 2 immune responses are dampened,[34–36] our findings imply the molecular processes through which sequence variation within noncoding elements at the *Ets1* locus predisposes individuals to allergic responses. These findings further establish a paradigm for understanding the importance of multi-enhancer hubs and transcription factor networks in quantitatively controlling gene expression in response to changes in cellular environment.

RESULTS

Exceptional enhancer connectivity at a type 2 immune disease-associated risk locus

We identified multi-enhancer hubs in T cells in an unbiased manner and leveraged human genetics to ascertain whether sequence variation within the top densely connected multi-enhancer hubs was linked to immune-mediated diseases. We reasoned that mapping multi-enhancer interactions in thymocytes, which represent T cells before any antigen exposure, can delineate critical regulatory units shared across T cell populations. Hence, we mapped enhancer interactions in double-positive (DP) thymocytes and used H3K27ac HiChIP,[22] which is a protein-centric assay for the 3D mapping of enhancer interactions.[37,38] We algorithmically searched for groups of densely connected multi-enhancers[21,22] (Figure 1A). The degree of enhancer connectivity was asymmetrical, reminiscent of asymmetrical histone acetylation at super-enhancers,[39,40] where only fewer than 18% of regulatory elements (2,372) spatially converged into "hyperconnected" multi-enhancer hubs defined based on the slope of 1 in the plot ranking their connectivity (Figure 1A; Table S1). Super-enhancers were enriched in hyperconnected hubs, suggesting extensive spatial connectivity among highly acetylated genomic elements (Figure 1B). Although not statistically significant, around 20% of hyperconnected hubs overlapped with annotated noncoding RNAs, and approximately 70% of hyperconnected hubs were characterized as architectural stripes[26,27] (Figure S1A). Overall, genes associated with T cell biology, including the "T cell receptor signaling pathway" and "adaptive immune system," were highly enriched at hyperconnected hubs (Figure 1C), thus suggesting that our analytical approach can prioritize regions harboring genes critical for T cell function.

The top hyperconnected locus in thymocytes encompassed the transcription factor *Bcl11b*[44] (Figure 1A). One of the major enhancer elements in this hyperconnected locus repositions from the peripheral lamina to the nuclear interior, a process which is required for T cell development and lymphomas.[45] The identification of *Bcl11b* as the most hyperconnected locus in T cells highlighted the sensitivity of our analytical approach in identifying genes with key biological roles in this lineage.

The second most hyperconnected multi-enhancer hub was detected at the locus encompassing two ETS-family transcription factors, *Ets1* and *Fli1*, and demonstrated conserved chromatin folding patterns between human and mouse T cells (Figures 1A, 1D, and 1E). While numerous SNPs associated with diverse diseases were distributed within the ~700 kbp region encompassing *ETS1* and *FLI1* in the human genome, variants associated with type 2 immune diseases, namely self-reported allergy,[32] asthma,[32] and atopic dermatitis,[33] were enriched within the ~25 kbp orthologous DNA segment that is ~250 kbp downstream of the *ETS1* promoter (SNPs in red, segment marked in yellow, Figure 1E). This regulatory segment was a major node of enhancer connectivity, overlapped with a long noncoding RNA annotated as *Gm27162*, and scored as a super-enhancer, and is hereafter referred to as "*Ets1*-SE" (red block, Figure 1D).

The unusual enrichment of type 2 immune disease-associated SNPs around the *Ets1*-SE element provided the rationale for us to test its functional relevance. Hence, we generated a mouse strain in which the 25 kbp *Ets1*-SE is deleted on the C57BL/6J background (Figure 1D). Since *ETS1* is required for the T cell lineage[46] and our multi-enhancer hub profiling was performed in DP T cells, we first assessed the effect of the *Ets1*-SE deletion on the expression of *Ets1* and *Fli1* in DP T cells using bulk RNA sequencing (RNA-seq). We found that *Fli1* expression did not change but *Ets1* expression was reduced by ~29% in *Ets1*-$SE^{-/-}$ DP T cells (Figure S1B). To visualize the genome reorganization of the *Ets1* locus in the absence of the *Ets1*-SE element in DP T cells, we used the "oligopaint" DNA fluorescence *in situ* hybridization (FISH) approach.[42,47] We painted 3 anchors of the *Ets1* multi-enhancer hub using probes from our earlier study[22]: a 50 kbp region spanning the *Fli1* promoter (E1), a 50 kbp region spanning the *Ets1* promoter and gene-body (E2), and a 50 kbp region spanning the 25 kbp *Ets1*-SE element and its downstream 25 kbp region (E3) (Figure 1D). We found that the average spatial distance between the *Ets1* promoter (E2) and proximal region to the *Ets1*-SE (E3) increased in *Ets1*-$SE^{-/-}$ compared with wild-type DP T cells in a mono-allelic manner (Figures 1F–1H). Moreover, multi-enhancer interactions (or 3D cliques) where all three regulatory elements converged into a hub in the same cell were detected in 2 times fewer alleles in *Ets1*-$SE^{-/-}$ compared with wild-type DP T cells, suggesting that the *Ets1*-SE deletion can rewire the *Ets1* locus (Figure S1C). Representative individual cells from wild-type and *Ets1*-$SE^{-/-}$ mice further corroborated the mono-allelic spatial localization of the *Ets1* promoter (E2) and *Ets1*-SE (E3) (Figures 1H and S1D). Together, our imaging experiments in DP T cells suggested the reorganization of the *Ets1* multi-enhancer hub in the absence of *Ets1*-SE.

Please cite this article in press as: Chandra et al., Quantitative control of *Ets1* dosage by a multi-enhancer hub promotes Th1 cell differentiation and protects from allergic inflammation, Immunity (2023), https://doi.org/10.1016/j.immuni.2023.05.004

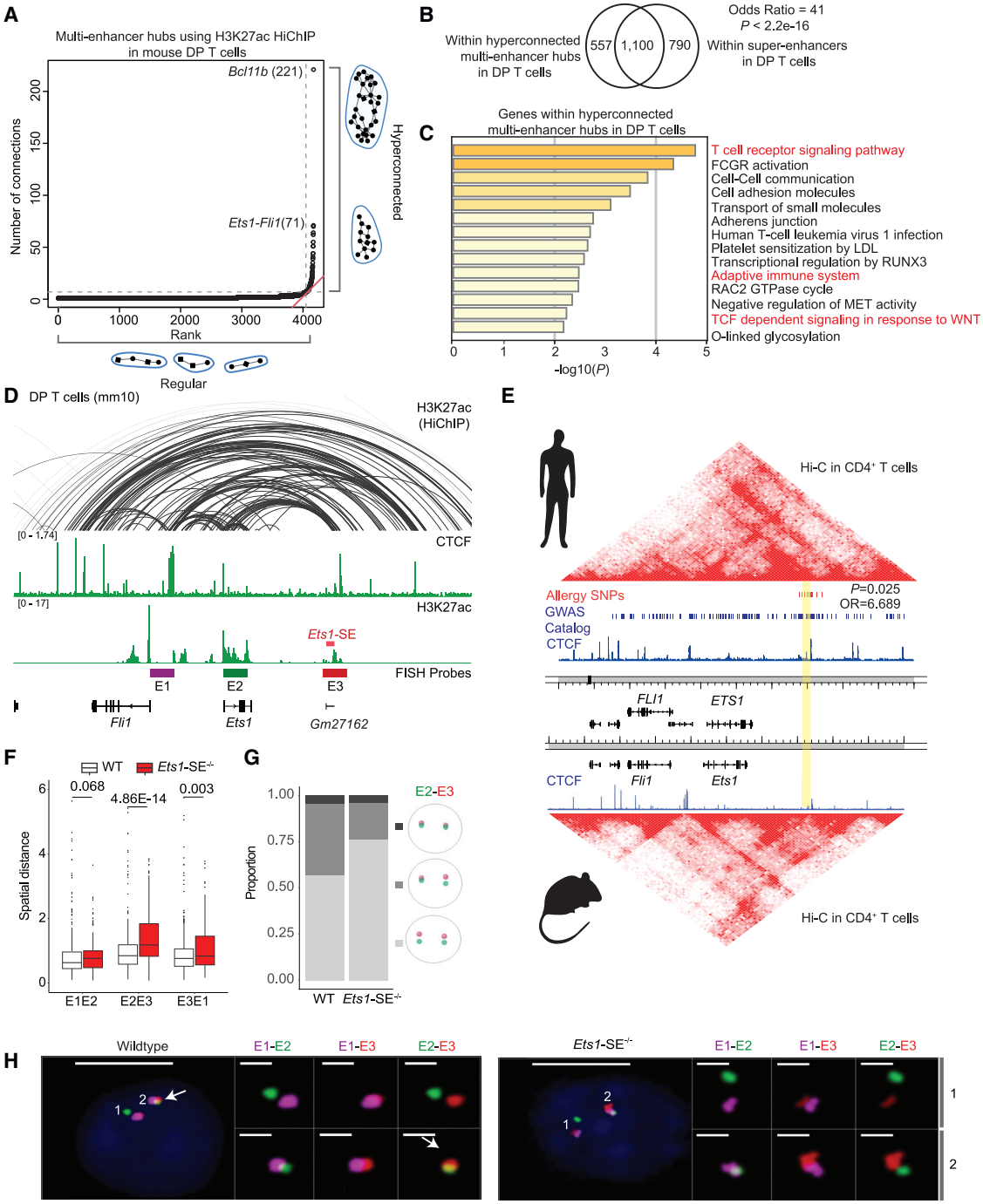

Figure 1. Exceptional enhancer connectivity at the *Ets1-Fli1* locus

(A) Plot depicts ranking versus number of connections in multi-enhancer hubs also referred to as 3D cliques[21,22] detected in double-positive (DP) T cells using H3K27ac HiChIP measurements generated in our previous study.[22] Hyperconnected multi-enhancer hubs are defined as the ones above the elbow of the total connectivity ranking. Top two hyperconnected multi-enhancer hubs *Bcl11b* and *Ets1-Fli1* are labeled. The number of interactions in each hub is provided in parentheses.

(B) Venn-diagram depicts the overlaps of genomic regions within hyperconnected multi-enhancer hubs detected using H3K27ac HiChIP when compared with super-enhancers defined by H3K27ac ChIP-seq in DP T cells. Super-enhancers were defined based on H3K27ac ChIP-seq in DP T cells as described before.[39] Odds ratio and Fisher's exact test were used for statistical analysis.

(C) Bar plot demonstrates the significance of Gene Ontology terms enriched in genes encompassing multi-enhancer hubs. Metascape[41] was used for Gene Ontology analysis. Terms relating to immune response pathways are marked in red.

(legend continued on next page)

Please cite this article in press as: Chandra et al., Quantitative control of *Ets1* dosage by a multi-enhancer hub promotes Th1 cell differentiation and protects from allergic inflammation, Immunity (2023), https://doi.org/10.1016/j.immuni.2023.05.004

Ets1-SE is dispensable for T cell development but required for *in vitro* Th1 differentiation

We next examined whether *Ets1*-SE deletion could lead to any phenotypic change in T cell development or T cell differentiation. Despite partial changes in the *Ets1* level and genome reorganization in DP T cells, T cell development remained intact in *Ets1*-SE$^{-/-}$ mice as the proportion of cells in the different thymic T cell developmental stages as well as the numbers of natural regulatory T cells (nTregs) were not significantly different when compared with wild-type mice (Figures 2A and S1E–S1G). At steady state, the majority of CD4$^+$ and CD8$^+$ T cell populations in peripheral tissues remained comparable between wild-type and *Ets1*-SE$^{-/-}$ mice (Figures S2H–S2J), apart from a moderate reduction in CD4$^+$ T cell numbers in the lungs (Figure 2B). Thus, perturbation of the hyperconnected *Ets1* locus was tolerated during T cell development.

The concentration of genetic variants associated with dysregulated type 2 immune responses within *Ets1*-SE implies a link between this region and CD4$^+$ T differentiation, which is a process mediated by changes in the extracellular cytokine milieu evoked by pathogenic stimuli.[48] We next explored whether perturbation in the *Ets1* multi-enhancer hub affected the capacity of CD4$^+$ T cells to differentiate into distinct T helper functional subsets *in vitro*.[34] Strikingly, naive CD4$^+$ T cells from *Ets1*-SE$^{-/-}$ mice had a significantly reduced capacity to differentiate into interferon-gamma (IFNγ) producing Th1 cells when compared with wild-type counterparts (Figure 2C). By contrast, Th2, Th17, and induced Treg (iTreg) differentiation measured by IL-13, IL-17, and FoxP3 expression, respectively, remained comparable between wild-type and *Ets1*-SE$^{-/-}$ CD4$^+$ T cells (Figures 2C and 2D). Thus, our results suggest that the *Ets1*-SE element is required for CD4$^+$ Th1 differentiation *in vitro*.

Mice lacking *Ets1*-SE are protected from Th1-mediated colitis but demonstrate overt allergic responses

To study the *in vivo* relevance of the *Ets1*-SE region, we tested the capacity of *Ets1*-SE$^{-/-}$ CD4$^+$ T cells to induce colitis using a well-established adoptive transfer Th1-driven model.[49] To do so, we adoptively transferred CD4$^+$CD45RB^{high} T cells from wild-type or *Ets1*-SE$^{-/-}$ mice into *Rag1*$^{-/-}$ mice and monitored their body weights as well as colitis development for 6 weeks (Figure 3A). As expected,[49] *Rag1*$^{-/-}$ mice that received wild-type CD4$^+$ T cells lost ~10% of their initial body weights by week 6 post-T cell transfer while *Rag1*$^{-/-}$ mice that received *Ets1*-SE$^{-/-}$ CD4$^+$ T cells steadily maintained their body weights (Figure 3B). In concordance, *Rag1*$^{-/-}$ mice that received *Ets1*-SE$^{-/-}$ CD4$^+$ T cells had significantly longer colon lengths and reduced severity in colonic histopathology when compared with wild-type T cell transfer, thus indicating that Th1-driven colon inflammation was drastically reduced in presence of *Ets1*-SE$^{-/-}$ CD4$^+$ T cells (Figures 3C–3E and S2A).

To evaluate the functional profiles of CD4$^+$ T cells in *Rag1*$^{-/-}$ recipient mice, we isolated CD4$^+$ T cells from the colon lamina propria (cLP) and spleen of these animals at least 6 weeks after the CD4$^+$CD45RB^{high} T cell transfers and measured the frequency and numbers of Th1, Th2, Th17, and Treg populations. In concordance with a decrease in the capacity of *Ets1*-SE$^{-/-}$ CD4$^+$ T cells to differentiate into IFNγ-producing Th1 cells, *Rag1*$^{-/-}$ mice that received wild-type CD4$^+$ T cells had significantly higher total numbers of CD4$^+$ T cells in the cLP and spleen as compared with *Rag1*$^{-/-}$ mice that received *Ets1*-SE$^{-/-}$ CD4$^+$ T cells (Figures 3F and 3G). Moreover, numbers of Granzyme B- and IFNγ-producing CD4$^+$ T cells were lower in *Ets1*-SE$^{-/-}$ injected *Rag1*$^{-/-}$ animals as compared with wild type (Figures 3F–3H), while numbers of Th2 or Th17 cells remained comparable (Figure 3F). Of note, our analysis revealed that there were no significant differences in total FoxP3$^+$ or T-bet$^+$ FoxP3$^+$ CD4$^+$ T cells in the spleen or the cLP of *Rag1*$^{-/-}$ mice injected with wild-type or *Ets1*-SE$^{-/-}$ cells (Figure S2B), suggesting that the decreased frequencies of CD4$^+$ Th1 cells as a result of *Ets1*-SE deficiency were not likely caused by significant alterations in the Treg population. Hence, *Ets1*-SE in CD4$^+$ T cells is specifically required for Th1 differentiation *in vivo* in the context of a Th1-induced colitis model.

IFNγ production by Th1 cells is a critical mechanism that dampens Th2 responses.[34–36] Since several SNPs associated with allergic diseases are clustered around the *Ets1*-SE element, we postulated that compromised Th1 differentiation in *Ets1*-SE$^{-/-}$ mice can lead to enhanced allergic responses *in vivo*. Hence, we challenged wild-type and *Ets1*-SE$^{-/-}$ mice with house dust mite (HDM) extracts for 5 consecutive days after an initial exposure and quantified immune cell infiltration and type 2 cytokine production in the lungs 17 days after the initial exposure

(D) The genome browser view demonstrates H3K27ac and CTCF ChIP-seq, as well as H3K27ac HiChIP 3D interactions at the *Ets1-Fli1* locus in DP T cells, and the exact genomic location of E1–E3 probes used for oligopaint DNA-FISH. The 25 kbp super-enhancer which is the focus of this study is called *Ets1*-SE and is marked in red. FISH probes depicted in the browser view include E1 (enhancer upstream of *Ets1* and proximal to *Fli1* promoter, magenta), E2 (*Ets1* promoter and gene-body, green), and E3 (*Ets1*-SE and a 25 kbp enhancer downstream of *Ets1*-SE, red), representing the three independent 50 kbp genomic regions for which oligopaint probes were designed.

(E) Heatmaps demonstrate contact-frequency maps measured by Hi-C in CD4$^+$ T cells in humans and mice. ChIP-seq tracks demonstrate CTCF binding in human CD4$^+$ T cells and mouse DP T cells. SNPs associated with asthma and allergic diseases highlighted in red were curated from the GWAS catalog and meta-analysis studies for allergy, asthma, and atopic dermatitis.[32,33] Blue bars demonstrate statistically significant GWAS SNPs associated with diverse traits. The orthologous human coordinate of *Gm27162* is highlighted in yellow (chr11:128,303,536-128,330,986). P value and odds ratio were estimated by Fisher's exact test.

(F) Boxplots depict the pairwise spatial distance formed between E1, E2, and E3 probes (Mann-Whitney U test). Oligopaint 3D FISH[42,43] in 428 and 460 thymocytes were imaged using widefield microscopy from one wild-type and one *Ets1*-SE$^{-/-}$ mouse, respectively. Spots for each probe in oligopaint 3D FISH data were analyzed in a semi-manual manner (STAR Methods).

(G) Divided bar plots demonstrating the proportion of mono vs. biallelic spatial contacts for E2 and E3 probes, in wild-type and *Ets1*-SE$^{-/-}$ cells. Only cells in which both alleles of both probes were detected, were used (112 wild-type cells and 53 *Ets1*-SE$^{-/-}$ cells). The distance cutoff used for E2 and E3 spatial contact was 0.7 μm. Pale gray represents no allele showing spatial contact, gray represents mono-allelic, and dark gray represents bi-allelic contacts.

(H) Representative images of the oligopaint FISH probes hybridization in one wild-type and one *Ets1*-SE$^{-/-}$ thymocytes, with the magnification of pairwise contacts for each allele. DAPI: blue, E1: magenta, E2: green, E3: red. Scale bars in whole cell: 5 μm and scale bars in magnification of allele: 1 μm. The white arrow represents the spatial overlap between E2 and E3.

Please cite this article in press as: Chandra et al., Quantitative control of *Ets1* dosage by a multi-enhancer hub promotes Th1 cell differentiation and protects from allergic inflammation, Immunity (2023), https://doi.org/10.1016/j.immuni.2023.05.004

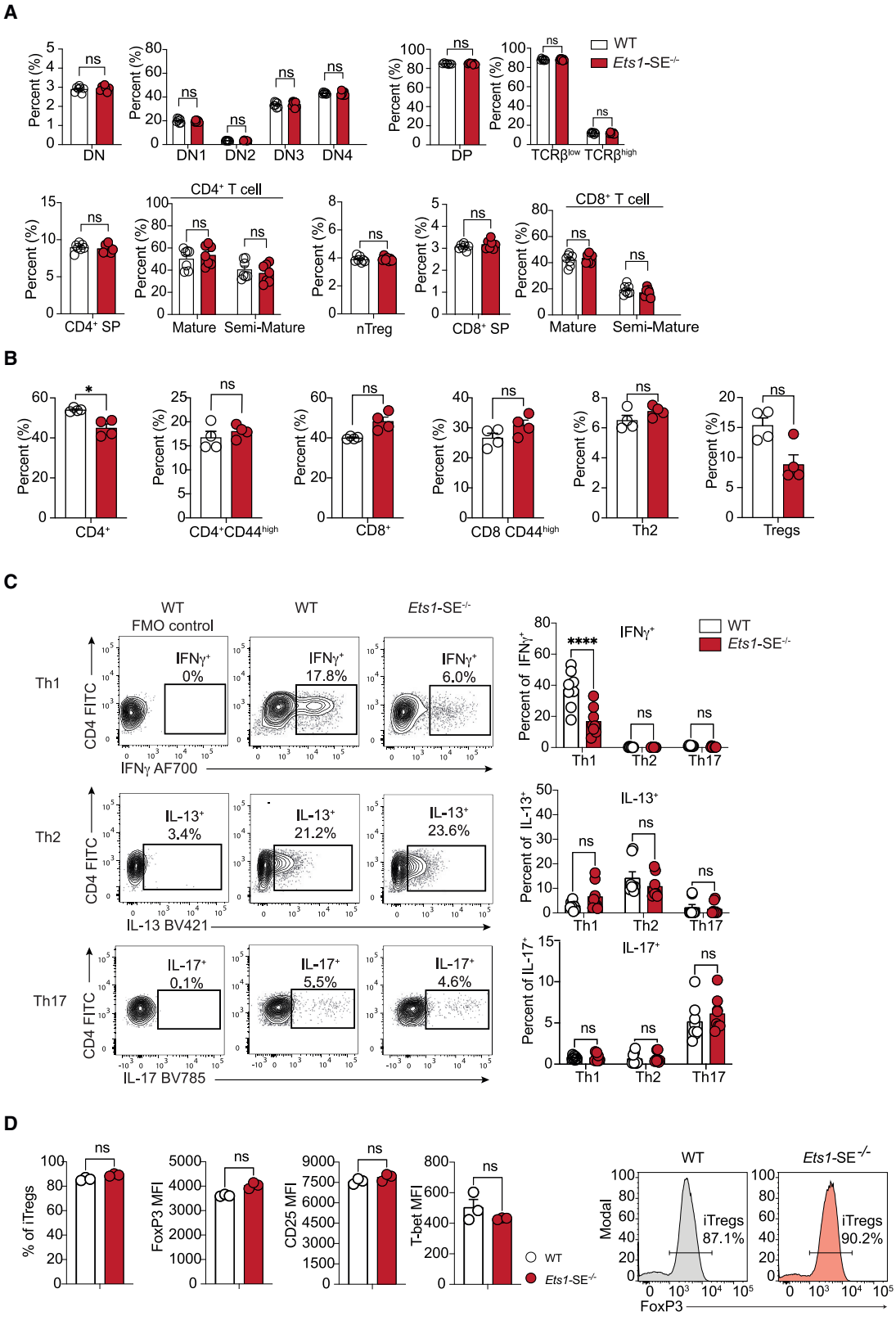

(legend on next page)

Please cite this article in press as: Chandra et al., Quantitative control of *Ets1* dosage by a multi-enhancer hub promotes Th1 cell differentiation and protects from allergic inflammation, Immunity (2023), https://doi.org/10.1016/j.immuni.2023.05.004

(Figure 3I). We found a significantly higher number of infiltrating CD4$^+$ and CD8$^+$ T cells in the lungs of *Ets1*-SE$^{-/-}$ animals compared with wild-type counterparts (Figure 3J). Notably, we observed dramatically increased numbers of eosinophils and Th2 cells in HDM-challenged *Ets1*-SE$^{-/-}$ mice, a key signature of over-active type 2 responses (Figure 3J). Moreover, *Ets1*-SE$^{-/-}$ mice also showed a significantly higher number of IL-5$^+$-producing Th2 cells during HDM-induced allergic airway inflammatory responses (Figure 3K). We did not observe any major differences in the frequencies or numbers of FoxP3$^+$ CD4$^+$ T cells, T-bet$^+$ FoxP3$^+$ CD4$^+$ T cells, or IFNγ-producing Th1 cells (Figures S2C and S2D). These results suggest that in the context of HDM-induced allergic airway inflammatory responses, *Ets1*-SE$^{-/-}$ CD4$^+$ T cells might have an increased intrinsic capacity to differentiate into Th2 cells. However, we cannot fully rule out the possibility that the *Ets1*-SE has an important role in other yet-to-be-identified immune cells that are critical for the expansion and maintenance of Th2 cells during allergic airway inflammatory responses.

Transcriptional outputs of Th1 cells depend on *Ets1*-SE

Considering the strong *in vivo* phenotype in the absence of *Ets1*-SE, we next measured changes in transcriptional outputs of CD4$^+$ T helper cells using RNA-seq. At the bulk level, *Ets1* expression was reduced by ~27% in *Ets1*-SE$^{-/-}$ Th1 cells but *Fli1* expression remained intact (Figure 4A). Moreover, the expression of 33 genes was reduced while the expression of 51 genes increased in *Ets1*-SE$^{-/-}$ Th1 cells (Figure 4B; Table S2). Strikingly, *Ets1*-SE deletion had a specific effect on the Th1 gene expression program, with Th1 signature genes, such as *Ifng*, selectively and significantly demonstrating reduced expression in *Ets1*-SE$^{-/-}$ Th1 cells compared with wild-type counterparts (Figure 4B) while Th2 signature genes were selectively upregulated in *Ets1*-SE$^{-/-}$ cells polarized under Th1 condition (Figure S3A). Unlike the Th1-specific effect of *Ets1*-SE, deletion of this regulatory element did not change the transcriptional landscape of Th2 cells (Figure S3B). Of note, the effect of *Ets1*-SE deletion on the expression level of *Ets1* and the number of differentially expressed genes was more pronounced in naive CD4$^+$ T cells (Figures 4A, S3C, and S3D). The *Ets1*-SE-deregulated genes in naive T cells were enriched with interferon-associated Gene Ontology, for example, *Ifit3*, implying the role of *Ets1*-SE in controlling the baseline expression of interferon genes (Figure S3F). Notably, *Ets1*-SE did not control the expression of cytokine receptors such as *Il12ra, Il4ra*, or *Il5ra* in naive T cells (Table S3). Together, the partial reduction in *Ets1* expression may cause a significant and specific decrease in the Th1-associated gene expression program.

We next examined the chromatin accessibility landscape of Th1 cells using bulk assay for transposase-accessible chromatin with sequencing (ATAC-seq) and found only a few genomic elements to be differentially accessible between wild-type and *Ets1*-SE$^{-/-}$ Th1 cells (Figure S4A). Similarly, a small number of genomic regions demonstrated significant alterations in histone acetylation as measured by H3K27ac cleavage under targets & release using nuclease (CUT&RUN[50]) in *Ets1*-SE$^{-/-}$ compared with wild-type Th1 cells (Figure S4B). Hence, we did not find strong evidence for the active enhancer landscape of Th1 cells to be dependent on *Ets1*-SE using these bulk measurements. Examining the binding of transcription factors within accessible chromatin regions of *Ets1*-SE suggested STAT1, STAT4, STAT3, STAT5a, and T-bet as potential upstream regulators of this locus in response to changes in the cytokine environment (Figure S4C). In line with transcriptional profiling, the chromatin accessibility landscapes of wild-type and *Ets1*-SE$^{-/-}$ Th2 cells were virtually indistinguishable (Figure S4D). Notably, the *Ets1*-SE deletion led to major changes in the chromatin accessibility landscape of naive T cells (Figures S4E–S4I). We also found that the *Ets1*-SE-dependent open chromatin regions in naive T cells had a low level of accessibility in differentiated Th1 cells, suggesting a distinct effect of *Ets1*-SE on the naive state (Figures S4G–S4I). Of note, the long noncoding RNA *Gm27162* demonstrated its highest expression and strongest chromatin accessibility in naive and Th1 cells (Figures S4J–S4K). Altogether, the analysis of bulk data suggests that the Th1-specific enhancer landscape was largely independent of the *Ets1*-SE element.

Although bulk RNA-seq measurements implied a link between *Ets1*-SE, the *Ets1* expression level, and transcriptional outputs of Th1 cells, it remained unclear whether the disruption of *Ets1*-SE can (1) reduce the *Ets1* expression level on a per-cell basis and thus leading to a uniform reduction across individual cells or (2) reduce the frequency of high *Ets1* expressing cells. We next used single-cell multiomics profiling[51] and generated joint single-cell RNA- and single-cell ATAC-seq measurements in CD4$^+$ T cells from wild-type and *Ets1*-SE$^{-/-}$ mice at two different

Figure 2. *Ets1*-SE is dispensable for thymic T cell generation but is required for CD4$^+$ Th1 differentiation

(A) Plots demonstrate the percentage of cells defined by flow cytometry analysis in the thymus from age-matched wild-type and *Ets1*-SE$^{-/-}$ female mice. Data are representative of three independent experiments. Each dot represents an individual mouse (wild type, n = 7, and *Ets1*-SE$^{-/-}$, n = 7). Error bars, SEM; and p: ns, not significant, (double-negative [DN], double-positive [DP], nTregs, CD4$^+$/CD8$^+$ SP: Mann-Whitney U test; DN1–DN4, TCRβ$^{low/high}$, semi-mature/mature CD4$^+$/CD8$^+$: two-way ANOVA with multiple comparisons and Bonferroni correction).

(B) Plots demonstrate percentages of cells defined by flow cytometry analysis in the lungs. Frequencies at steady state of T cells in the lungs from age-matched wild-type and *Ets1*-SE$^{-/-}$ male mice. Data are representative of two independent experiments. Each dot represents an individual mouse (wild type, n = 4, and *Ets1*-SE$^{-/-}$, n = 4). Error bars, SEM; and p: ns, not significant, *p ≤ 0.05 (Mann-Whitney U test).

(C) (Left) Representative flow cytometry contour plot of naive CD4$^+$ T cells from wild-type or *Ets1*-SE$^{-/-}$ mice cultured under Th1, Th2, or Th17 polarizing conditions for 6 days. Unstained wild-type cells are shown for each polarizing condition as a negative control (wild-type FMO control). (Right) Frequencies of Th1 (IFNγ$^+$), Th2 (IL-13$^+$), or Th17 (IL-17$^+$) cytokines producing CD4$^+$ T cells cultured under Th1, Th2, or Th17 polarizing conditions for 6 days. Two independent experiments were pooled and repeated five times. Each dot represents an individual mouse (wild type, n = 8, and *Ets1*-SE$^{-/-}$, n = 8). Error bars, SEM; and p: ns, not significant, *p ≤ 0.05, **p ≤ 0.01, ***p ≤ 0.0005, ****p ≤ 0.0001 (two-way ANOVA with multiple comparisons and Bonferroni correction).

(D) (Left) Frequencies of induced Tregs (iTregs, FoxP3$^+$ CD4$^+$ cells) and mean fluorescence intensity (MFI) of FoxP3, CD25, and T-bet from naive CD4$^+$ T cells cultured under iTreg polarizing conditions for 3 days. (Right) Representative histogram of the proportion of FoxP3+ CD4$^+$ T cells 3 days after culturing in iTregs polarizing conditions. Data are representatives of two independent experiments. Each dot represents an individual mouse (wild type, n = 3, and *Ets1*-SE$^{-/-}$, n = 3). Error bars, SEM; and p: ns, not significant, *p ≤ 0.05, **p ≤ 0.01, ***p ≤ 0.0005, ****p ≤ 0.0001 (Mann-Whitney U test).

Please cite this article in press as: Chandra et al., Quantitative control of *Ets1* dosage by a multi-enhancer hub promotes Th1 cell differentiation and protects from allergic inflammation, Immunity (2023), https://doi.org/10.1016/j.immuni.2023.05.004

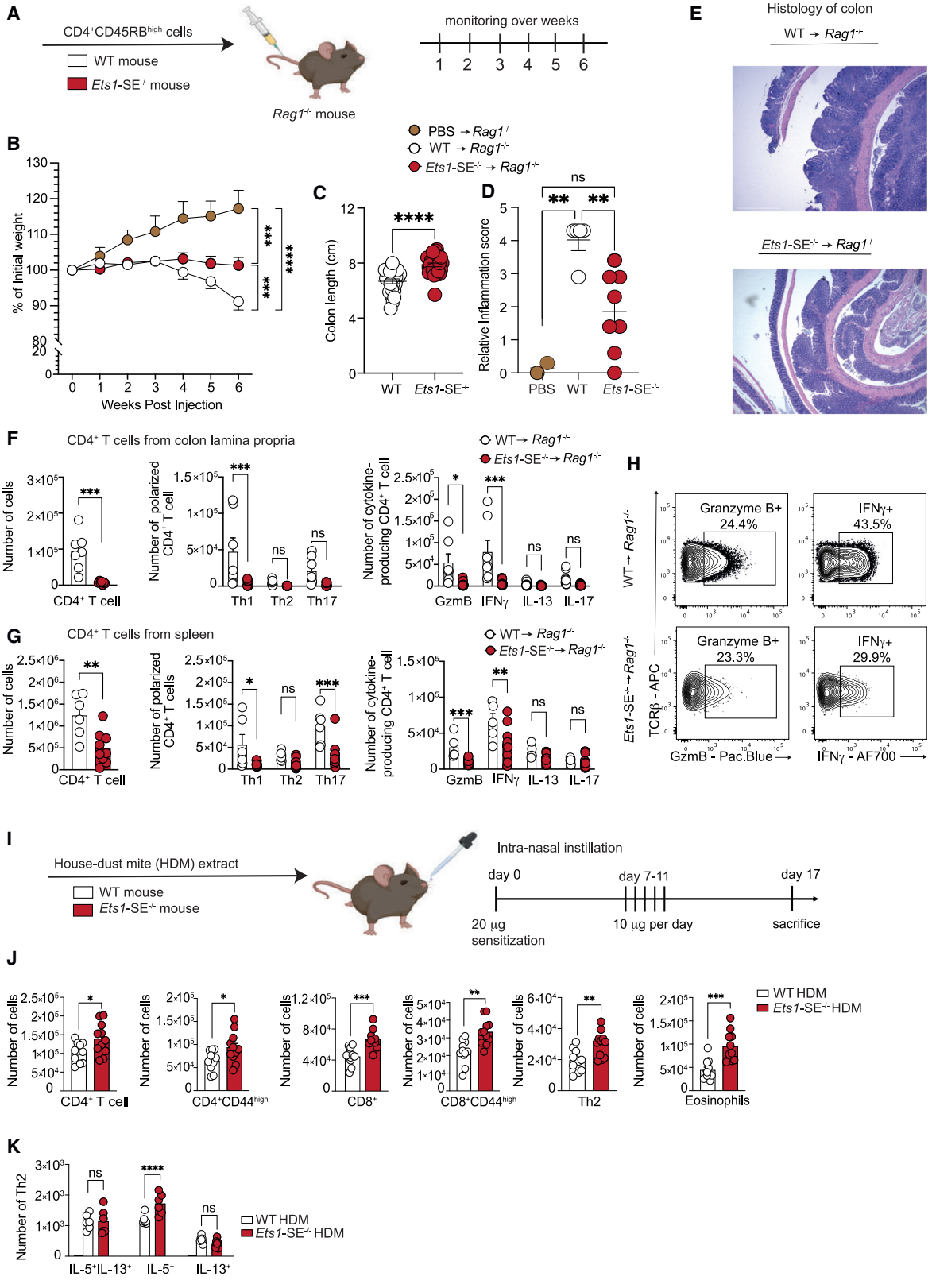

Figure 3. *Ets1*-SE deletion limits Th1-mediated inflammation *in vivo*

(A) Schematic of the CD45RB^{High}-induced colitis model. 1 ×10^6 FACS sorted TCRβ$^+$, CD4$^+$, CD45RB^{High} naive CD4$^+$ T cells from wild-type or *Ets1*-SE$^{-/-}$ were transferred into *Rag1*$^{-/-}$ recipients.

(legend continued on next page)

dynamic time points (days 1 and 6) after Th1 polarization *in vitro*. After quality control filtering (Figure S5A), we obtained a total of ~80,000 cells with comparable contributions from wild-type and *Ets1*-SE$^{-/-}$ mice using two technical replicates. We detected 9 distinct clusters using the weighted nearest neighbor analysis,[51] which incorporated both gene expression and chromatin accessibility measurements for the dimensionality reduction and clustering analysis (Figures 4D, 4E, and S5B). Relying on marker genes, we assigned clusters to four different CD4$^+$ T cell states: (1) the resting state (*Ccr7* and *Tcf7* expressing cells in clusters 0, 7), (2) the activated state (*Nrf4a1* and *Cd69* expressing cells in clusters 2, 3, 6), (3) the Th1 state (*Ifng* and *Tbx21* expressing cells in clusters 1, 4, 8) and (4) the proliferating Th1 state (*Ifng* and *Mki67* expressing cells in cluster 5) (Figures 4D, 4E, and S5B). Cells from both wild-type and *Ets1*-SE$^{-/-}$ T cells comprised these clusters with different frequencies (Figure 4F).

We next assessed the extent of variation in the *Ets1* mRNA level across individual cells. Focusing first on wild-type CD4$^+$ T cells revealed that the frequency of high *Ets1*-expressing cells was the largest in cells associated with the resting state and the *Ifng*-producing Th1 state (Figure 4G, gray violin plots). High *Ets1* expressing cells were not frequently detected in activated wild-type T cells representing low *Ifng* expressing cells 1 day after Th1 polarization. This reduction in frequencies of high *Ets1* expressing cells in the activated state is in line with previous studies suggesting the downregulation of *Ets1* level by T cell activation.[52] Strikingly, the dynamic increase of the *Ets1* level during Th1 polarization was impaired in *Ets1*-SE$^{-/-}$ cells (Figure 4G, red/pink violin plots). Collectively, the distributions of *Ets1* expression were comparable in individual cells from *Ets1*-SE$^{-/-}$ mice grouped into all four states (Figure 4G, red/pink violin plots). Quantitatively, the largest difference for *Ets1* expression between wild-type and *Ets1*-SE$^{-/-}$ cells occurred in proliferating Th1 cells, suggesting ~60% reduction in the *Ets1* level after *Ets1*-SE deletion. The simultaneous measurement of chromatin accessibility in the multiome assay across these clusters corroborated findings based on bulk ATAC-seq (Figure 4H). Together, our single-cell multiome profiling measurements suggest that deletion of *Ets1*-SE within the multi-enhancer hub impairs the ability of CD4$^+$ T cells to express high levels of *Ets1* in response to Th1 stimulation.

ETS1 dosage controls Th1 differentiation

We next assessed whether the partial reduction of *Ets1* was responsible for the compromised Th1 differentiation using two complementary dosage experiments. First, we used *Ets1* heterozygous mice (*Ets1*$^{fl/+}$*Cd4*^{cre}) that harbor a 50% reduction of *Ets1* transcript and protein levels in CD4$^+$ T cells. Second, we overexpressed the ETS1 protein in *Ets1*-SE$^{-/-}$ Th1 cells that carry a partial reduction of *Ets1* as compared with wild-type cells. Thus, using these *Ets1* dosage experiments, if the *Ets1* expression level

(B) Weight loss tracking of *Rag1*$^{-/-}$ mice as compared with PBS-injected control animals (three independent experiments, repeated four times). Dots represent the mean of individual mice (PBS, n = 5; wild type, n = 25; *Ets1*-SE$^{-/-}$, n = 27). Error bars, SEM; and p: ns, not significant, *p ≤ 0.05, **p ≤ 0.01, ***p ≤ 0.0005, ****p ≤ 0.0001 (two-way ANOVA; mixed-effect restricted maximum likelihood [REML] model with Fisher's LSD test).

(C) Quantification of colon length (cm) of *Rag1*$^{-/-}$ mice that received either wild-type or *Ets1*-SE$^{-/-}$ CD4$^+$ T cells (three independent experiments repeated four times). Dots represent the mean of individual mice (wild type, n = 25; *Ets1*-SE$^{-/-}$, n = 27). Error bars, SEM; and p: ns, not significant, *p ≤ 0.05, **p ≤ 0.01, ***p ≤ 0.0005, ****p ≤ 0.0001 (Mann-Whitney U test).

(D and E) Quantification of the histological score of paraffin-embedded colon rolls from *Rag1*$^{-/-}$ mice that received either wild-type or *Ets1*-SE$^{-/-}$ mice at week 6 post transfer and as compared with PBS-injected mice (control). Histological sections were obtained from two independent experiments and were scored in a blinded manner. Each dot represents an individual mouse (PBS, n = 2; wild type, n = 5; and Ets1-SE$^{-/-}$, n = 8). Error bars, SEM; and p: ns, not significant, *p ≤ 0.05, **p ≤ 0.01, ***p ≤ 0.0005, ****p ≤ 0.0001 (one-way ANOVA with multiple comparisons and Bonferroni correction). (E) Histological section of colon rolls stained with H&E of *Rag1*$^{-/-}$ mice that received either 1 × 10^6 FACS sorted TCR$^+$, CD4$^+$, CD45RB^{High} naive wild-type or *Ets1*-SE$^{-/-}$ CD4$^+$ T cells 6 weeks post-transfer. Scale bars, 100 μm; magnification = 100×.

(F) (Left) Quantification of infiltrating colon lamina propria (cLP) colitogenic CD4$^+$ T cells of *Rag1*$^{-/-}$ mice that received either wild-type or *Ets1*-SE$^{-/-}$ CD4$^+$ T cells. (Middle) Quantification of Th1 (T-bet$^+$), Th2 (GATA-3$^+$), Th17 (RORγ-t$^+$) CD4$^+$ T cells among infiltrating cLP CD4$^+$ T cells of *Rag1*$^{-/-}$ mice that received either wild-type or *Ets1*-SE$^{-/-}$ CD4$^+$ T cells. (Right) Quantification of Th1 (IFNγ$^+$), Th2 (IL-13$^+$), Th17 (IL-17$^+$), and Granzyme B (GzmB$^+$) producing CD4$^+$ T cells among infiltrating cLP CD4$^+$ T cells of *Rag1*$^{-/-}$ mice that received either wild-type or *Ets1*-SE$^{-/-}$ CD4$^+$ T cells. Two independent experiments were pooled. Dots represent an individual mouse (wild type, n = 7, and *Ets1*-SE$^{-/-}$, n = 7). Error bars, SEM; and p: ns, not significant, *p ≤ 0.05, **p ≤ 0.01, ***p ≤ 0.0005, ****p ≤ 0.0001 (CD4$^+$ T cells: Mann-Whitney U test; Th1/Th2/Th17/Treg and cytokines production: two-way ANOVA with multiple comparisons and Bonferroni correction).

(G) (Left) Quantification CD4$^+$ T cells in the spleen of *Rag1*$^{-/-}$ mice that received wild-type or *Ets1*-SE$^{-/-}$ CD4$^+$ T cells. (Middle) Quantification in the spleen of Th1 (T-bet$^+$), Th2 (GATA-3$^+$), and Th17 (RORγ-t$^+$) CD4$^+$ T cells of *Rag1*$^{-/-}$ mice that received either wild-type or *Ets1*-SE$^{-/-}$ CD4$^+$ T cells. (Right) Quantification of *ex vivo* stimulated splenic Th1 (IFNγ$^+$), Th2 (IL-13$^+$), Th17 (IL-17$^+$), and Granzyme B (Gzm B$^+$) producing CD4$^+$ T cells of *Rag1*$^{-/-}$ mice that received either wild-type or *Ets1*-SE$^{-/-}$ CD4$^+$ T cells. Data represent one experiment that was repeated three times. Dots represent an individual mouse (wild type, n = 7, and Ets1-SE$^{-/-}$, n = 7). Error bars, SEM; and p values: ns, not significant, *p ≤ 0.05, **p ≤ 0.01, ***p ≤ 0.0005, ****p ≤ 0.0001 (CD4$^+$ T cells: Mann-Whitney U test; Th1/Th2/Th17/Treg and cytokines production: two-way ANOVA with multiple comparisons and Bonferroni correction).

(H) Representative flow cytometry contour plot of Granzyme B- and IFNγ-producing *ex vivo* stimulated cLP CD4$^+$ T cells of *Rag1*$^{-/-}$ mice that received either wild-type or *Ets1*-SE$^{-/-}$ CD4$^+$ T cells.

(I) Schematic representation of the house dust mite (HDM) extract challenge. Arrows represent the days by which intranasal HDM was administered. Mice were euthanized 16 days after the initial sensitization and immune cell infiltration was checked. Two independent experiments were used to measure immune cell infiltration in the lung parenchyma.

(J) Quantification of lung parenchyma infiltrating CD4$^+$ T cells (TCRβ$^+$, CD4$^+$), activated CD4$^+$ T cells (TCRβ$^+$, CD4$^+$, CD44$^+$), CD8$^+$ T cells (TCRβ$^+$, CD8$^+$), activated CD4$^+$ T cells (TCRβ$^+$, CD8$^+$, CD44$^+$), CD4$^+$ Th2 cells (TCRβ$^+$, CD4$^+$, GATA-3$^+$), and eosinophils (MHC-II$^-$, Siglec-F$^+$) from wild-type or *Ets1*-SE$^{-/-}$ mice 16 days after HDM challenge. Two independent experiments were pooled. Each dot represents an individual mouse (wild type, n = 11, and *Ets1*-SE$^{-/-}$, n = 11). Error bars, SEM; and ns, not significant, *p ≤ 0.05, **p ≤ 0.01, ***p ≤ 0.0005, ****p ≤ 0.0001 (Mann-Whitney).

(K) Quantification of Th2 cell numbers from wild-type or *Ets1*-SE$^{-/-}$ mice producing IL-5, IL-13, or IL-5/IL-13 4 h after PMA and ionomycin stimulation. Data are representative of one independent experiment and repeated twice. Each dot represents an individual mouse (wild type, n = 6, and *Ets1*-SE$^{-/-}$, n = 6). Error bars, SEM; and p: ns, not significant, *p ≤ 0.05, **p ≤ 0.01, ***p ≤ 0.0005, ****p ≤ 0.0001 (two-way ANOVA with multiple comparison and Bonferroni correction).

Please cite this article in press as: Chandra et al., Quantitative control of *Ets1* dosage by a multi-enhancer hub promotes Th1 cell differentiation and protects from allergic inflammation, Immunity (2023), https://doi.org/10.1016/j.immuni.2023.05.004

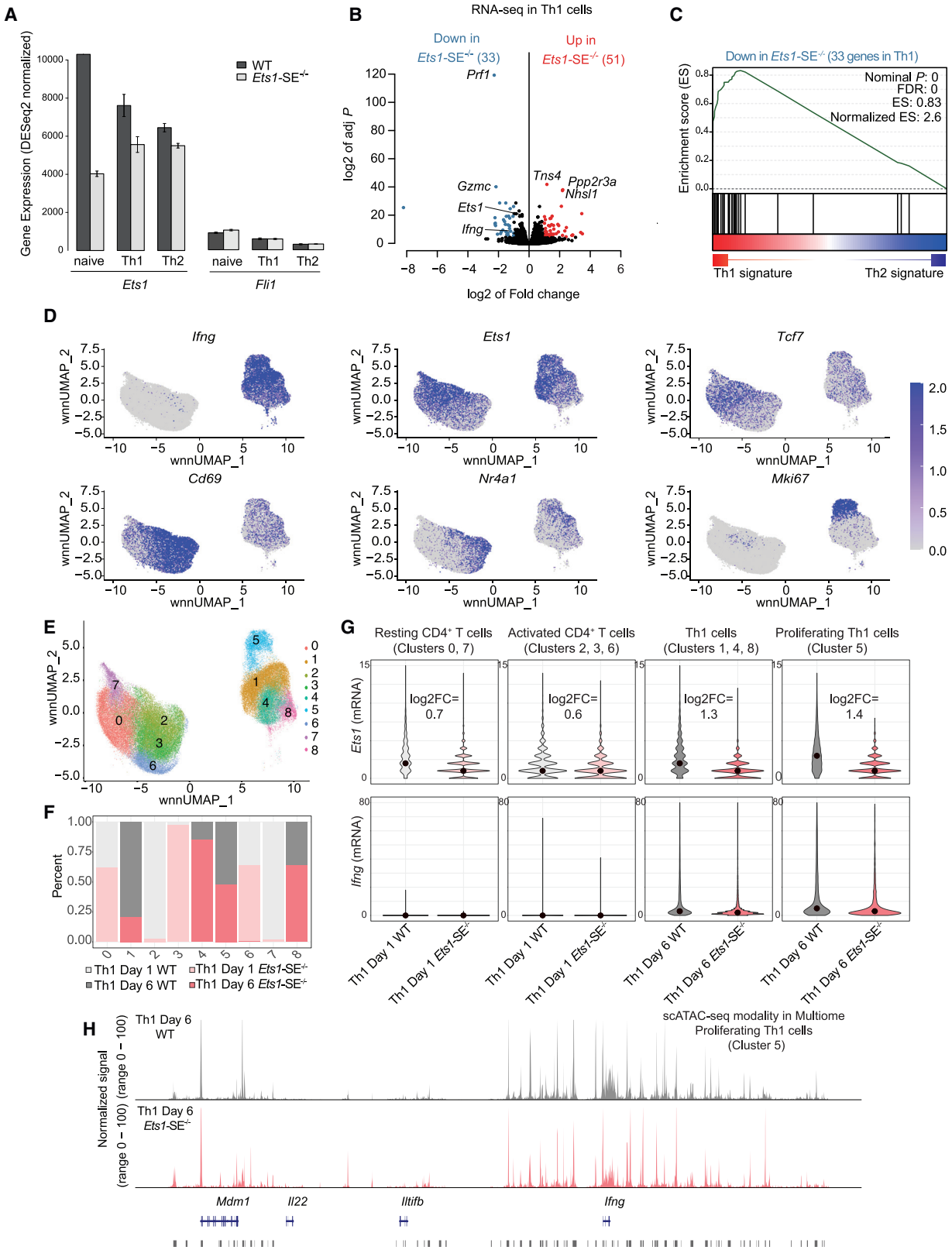

Figure 4. Reorganization of the multi-enhancer hub in the absence of the *Ets1*-SE element

(A) Barplot demonstrates normalized mRNA levels of *Ets1* and *Fli1* using bulk RNA-seq experiments in wild-type and *Ets1*-SE$^{-/-}$ naive CD4^{+} and *in vitro* polarized Th1 and Th2 cells performed in three replicates.

(legend continued on next page)

Please cite this article in press as: Chandra et al., Quantitative control of *Ets1* dosage by a multi-enhancer hub promotes Th1 cell differentiation and protects from allergic inflammation, Immunity (2023), https://doi.org/10.1016/j.immuni.2023.05.004

controls Th1 differentiation through the *Ets1*-SE element (in *cis*), we expect that cells carrying one copy of the *Ets1* gene, but an intact *Ets1*-SE region, would also fail to differentiate effectively toward the Th1 program. Moreover, we expect that the reconstitution of ETS1 in *Ets1*-SE$^{-/-}$ Th1 cells to the wild-type level can rescue optimal Th1 differentiation. We observed a significant loss of IFNγ expressing cells upon *in vitro* Th1 polarization of naive CD4$^+$ cells from *Ets1*$^{fl/+}$*Cd4*^{cre} mice when compared with wild-type counterparts (Figure 5A). Furthermore, the reconstitution of ETS1 expression into *Ets1*-SE$^{-/-}$ cells using retroviral transduction during *in vitro* Th1 polarization significantly increased the frequency of IFNγ expressing cells compared with empty-vector transduced cells (Figures 5B and 5C). Transcriptional profiling of *Ets1*-SE$^{-/-}$ Th1 cells with the ectopic expression of ETS1 also confirmed the selective rescue of Th1-signature genes (Figures 5D, S5C, and S5D). Together, *Ets1*-SE acts in *cis*, tuning a precise expression level of *Ets1* which is required for optimal Th1 differentiation.

Ets1 level controls the 3D genome topology of Th1 cells by recruiting CTCF

To assess whether *Ets1*-SE is required for the spatial localization of enhancers to Th1 signature genes, we created unbiased maps of long-range interactions in CD4$^+$ T helper cells using ultra-deep Hi-C.[53,54] Focusing on the genome organization of the *Ets1* locus in wild-type T cells, we found that the *Ets1*-SE demonstrated the strongest interaction with the *Ets1* gene locus in naive and CD4$^+$ Th1 cells, a trend which is consistent with the expression level of *Ets1* in these T cell subsets (Figures S5E and S5F). Comparing wild-type and *Ets1*-SE$^{-/-}$ Th1 cells revealed that compartments and topologically associating domains (TADs) were independent of *Ets1*-SE (Figures S5G and S5H). However, we observed extensive weakening of long-range interactions in *Ets1*-SE$^{-/-}$ as compared with wild-type Th1 cells (Figure S6A). Genes associated with Th1 biology including *Ifng* and *Il1r-Il18r* were located within loop domains with reduced interaction in *Ets1*-SE$^{-/-}$ compared with wild-type cells, suggesting the specific effect of *Ets1*-SE on Th1-specific genome topology (Figures S6B and S6C). Consistent with gene expression and chromatin accessibility measurements, the effect of the *Ets1*-SE deletion on long-range interactions was less pronounced in Th2 cells compared with the effect of this regulatory element on Th1 cells (Figure S6D).

To dissect whether changes in genome topology in *Ets1*-SE$^{-/-}$ Th1 cells were mediated by a reduction in the level of *Ets1* expression, we also measured long-range interactions using Hi-C in *Ets1* heterozygous (*Ets1*$^{fl/+}$*Cd4*^{cre}) Th1 cells, where the *Ets1*-SE sequence is intact. Remarkably, we detected an extensive similarity between *Ets1*-SE$^{-/-}$ and *Ets1*$^{fl/+}$*Cd4*^{cre} Th1 cells: 4,726 loops including interactions at the *Ets1* locus were weaker in both *Ets1*-SE$^{-/-}$ and *Ets1*$^{fl/+}$*Cd4*^{cre} Th1 cells compared with wild-type counterparts (Figures 6A–6C). The weaker interactions in *Ets1*-SE$^{-/-}$ Th1 cells at the *Ets1* locus were consistent with the oligopaint results in DP T cells, demonstrating an increased spatial distance among regulatory elements in *Ets1*-SE$^{-/-}$ cells (Figures 1F–1H). Thus, a precise level of *Ets1* expression controlled by the *Ets1*-SE element is required for the Th1-associated genome topology.

We next assessed whether the partial reduction of *Ets1* could modify the genome-wide occupancy of ETS1 protein and if there was any direct evidence for ETS1 binding affecting Th1-associated long-range interactions. We therefore mapped the global binding pattern of ETS1 protein in biological replicates of Th1 cells using CUT&RUN[50] (Figure S6E). Overall, we detected more than 27,000 genomic regions bound by ETS1 in wild-type Th1 cells enriched with the canonical ETS recognition motif and found ~33% occupancy at promoter regions, suggesting the high quality of our CUT&RUN measurements (Figures S6E and S6F; Table S4). Considering the unexpected effect of the *Ets1* expression level on the 3D genome organization of Th1 cells (Figures 6A–6C), we next measured the genome-wide occupancy of CTCF using CUT&RUN and found that more than 50% of ETS1 binding events co-occurred at CTCF-bound sites in Th1 cells (Figure S6G). Moreover, ETS1 and CTCF co-binding was detected at a significant proportion of Th1-associated loop anchors, suggesting the potential cooperation of ETS1 and CTCF in establishing the 3D genome topology of Th1 cells (Figure 6D). Although it has been reported that the complete deletion of *Ets1* in CD4$^+$ T cells reduces the expression of CTCF,[55] the CTCF mRNA level was intact in *Ets1*-SE$^{-/-}$ Th1 cells (Table S2A). To further understand how the reduced expression of *Ets1* weakened long-range interactions in *Ets1*-SE$^{-/-}$ Th1 cells, we compared ETS1 and CTCF occupancies in wild-type and *Ets1*-SE$^{-/-}$ Th1 cells. While the majority of ETS1 and CTCF binding events were not sensitive to the *Ets1* expression level, 988 genomic regions demonstrated a coordinated loss of both ETS1 and CTCF binding in *Ets1*-SE$^{-/-}$ compared with wild-type Th1 cells (Figure 6E; Table S5). In addition, 364 genomic regions demonstrated a coordinated gain of both proteins in *Ets1*-SE$^{-/-}$ compared with wild-type Th1 cells (Figure 6F). The subset of ETS1-CTCF co-occupied regions with a coordinated loss of both proteins in *Ets1*-SE$^{-/-}$ Th1 cells demonstrated lower ETS1 and CTCF occupancy compared with the majority of unaffected binding events in wild-type Th1 cells, implying the overall sensitivity of these loci to the *Ets1* expression level (Figure S6H). Remarkably,

(B) Volcano plot demonstrates differential expression analysis of bulk RNA-seq experiments in wild-type and *Ets1*-SE$^{-/-}$ *in vitro* Th1 polarized cells studied at day 6. Three replicates were used to perform DESeq2 analysis and $|\log_2 FC|>1$, adjusted $p < 0.05$ were used to determine differentially expressed genes.

(C) Pre-ranked gene set enrichment analysis (GSEA) depicts the enrichment of gene set for downregulated genes in *Ets1*-SE$^{-/-}$ compared with wild-type Th1 cells. The pre-ranked genes were defined based on DESeq2 analysis of wild-type Th1 and Th2 cells.

(D and E) Weighted nearest neighbor UMAP (wnnUMAP) projection, which uses both gene expression and chromatin accessibility measurements for dimensionality reduction and clustering of single-cell multiomics analysis on wild-type and *Ets1*-SE$^{-/-}$ days 1 and 6 Th1 cells using technical replicates, showing mRNA level of *Ifng*, *Ets1*, *Tcf7*, *Cd69*, *Nr4a1*, and *Mki67* in each cell. (E) Cluster numbers across wnnUMAP.

(F) Barplots showing the composition of each of the 9 clusters including proportion and contribution from each of the four conditions: wild-type and *Ets1*-SE$^{-/-}$ Th1 after days 1 and 6 of *in vitro* cluster. Biological replicates were performed and cells were pooled.

(G) Violin plots showing the expression levels of *Ets1* and *Ifng* across individual wild-type and *Ets1*-SE$^{-/-}$ cells within clusters annotated as resting CD4$^+$ T cells (clusters 0 and 7), activated CD4$^+$ T cells (clusters 2, 3, and 6), Th1 cells (clusters 1, 4, and 8), and proliferating Th1 cells (cluster 5).

(H) Representative pseudo-bulk ATAC-seq tracks from scATAC-seq modality in multiome of proliferating Th1 cells (cluster 5), showing comparable chromatin accessibility between wild-type and *Ets1*-SE$^{-/-}$ Th1 cells.

Please cite this article in press as: Chandra et al., Quantitative control of *Ets1* dosage by a multi-enhancer hub promotes Th1 cell differentiation and protects from allergic inflammation, Immunity (2023), https://doi.org/10.1016/j.immuni.2023.05.004

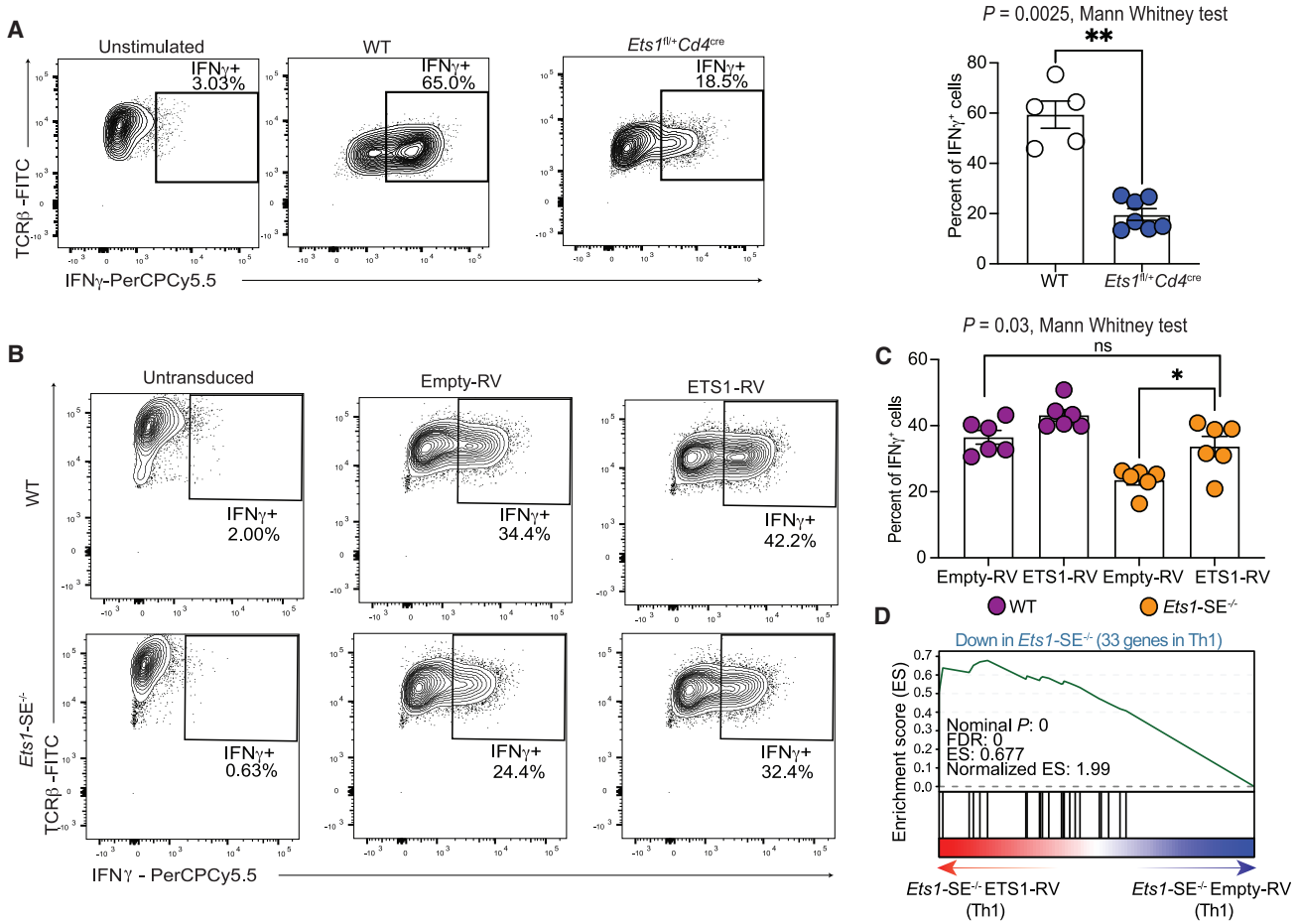

Figure 5. ETS1 dosage controls Th1 differentiation

(A) Flow cytometry results demonstrating the frequency of IFNγ expressing cells under unstimulated (left) and *in vitro* Th1 polarization for 6 days in wild-type (middle) and *Ets1* heterozygous mice (*Ets1*$^{fl/+}$*Cd4*^{cre}) (right). The right panel shows bar plot of average results from two independent experiments. Each dot represents an individual mouse. Statistical significance was evaluated using a non-parametric Mann-Whitney test. **p = 0.0025.

(B and C) (B) Flow cytometry results demonstrating the frequency of IFNγ expressing cells when naive CD4$^+$ T cells were retrovirally transduced with empty vector (Empty-RV) or ETS1 expressing vector (ETS1-RV) and were polarized under *in vitro* Th1-differentiating conditions for 6 days. The panel shows representative contour plots, and (C) shows the bar plot of average results from two independent experiments. Each dot represents an individual mouse. Significance was tested using a non-parametric Mann-Whitney test. *p = 0.03.

(D) Pre-ranked gene set enrichment analysis (GSEA) depicts the enrichment of the downregulated genes in *Ets1*-SE$^{-/-}$ compared with wild-type Th1 cells as gene set. The pre-ranked genes based on DESeq2 analysis of *Ets1*-SE$^{-/-}$ cells transduced with empty-vector and ETS1-expressing vector. Three technical replicates were used for DESeq2 analysis.

the ETS-RUNX (Runt-related transcription factor) cooperative binding motif, which has been characterized as the T cell activation signature of ETS1 binding,[56,57] was enriched at genomic regions which were sensitive to the *Ets1* level (Figures S6I and S6J). STAT2 and Tbox motifs which are recognition sites for Th1-specific transcription factors T-bet and STAT2 were also enriched at these ETS1-CTCF lost sites, suggesting the potential cooperation of ETS1 with these proteins (Figures S6I and S6J). Remarkably, genomic regions whose ETS1 and CTCF co-occupancy were sensitive to the *Ets1* level demonstrated altered long-range interactions in *Ets1*-SE$^{-/-}$ Th1 cells (Figures 6G and 6H). These results indicate that a precise level of ETS1 protein was required for CTCF occupancy and the 3D long-range interactions for Th1 regulatory elements. Altogether, the hyperconnectivity of the *Ets1-Fli1* locus controlled the expression level of *Ets1* which was dispensable for the active enhancer signature but required for the Th1-specific DNA folding through recruitment of CTCF. This specific deficit in genome folding due to a partial reduction of *Ets1* led to compromised Th1 differentiation and allergic responses *in vivo*.

DISCUSSION

Here, we interrogated the functional relevance of a 3D structure referred to as a multi-enhancer hub in the context of T cell differentiation. Systematic prioritization of 3D genome interactions in mouse T cells ranked the *Ets1-Fli1* region as the second most hyperconnected locus after the *Bcl11b* region, with an unusual degree of enhancer connectivity. This multi-enhancer locus was conserved in human T cells and represented a hotspot for SNPs associated with allergic diseases. To better understand

Please cite this article in press as: Chandra et al., Quantitative control of *Ets1* dosage by a multi-enhancer hub promotes Th1 cell differentiation and protects from allergic inflammation, Immunity (2023), https://doi.org/10.1016/j.immuni.2023.05.004

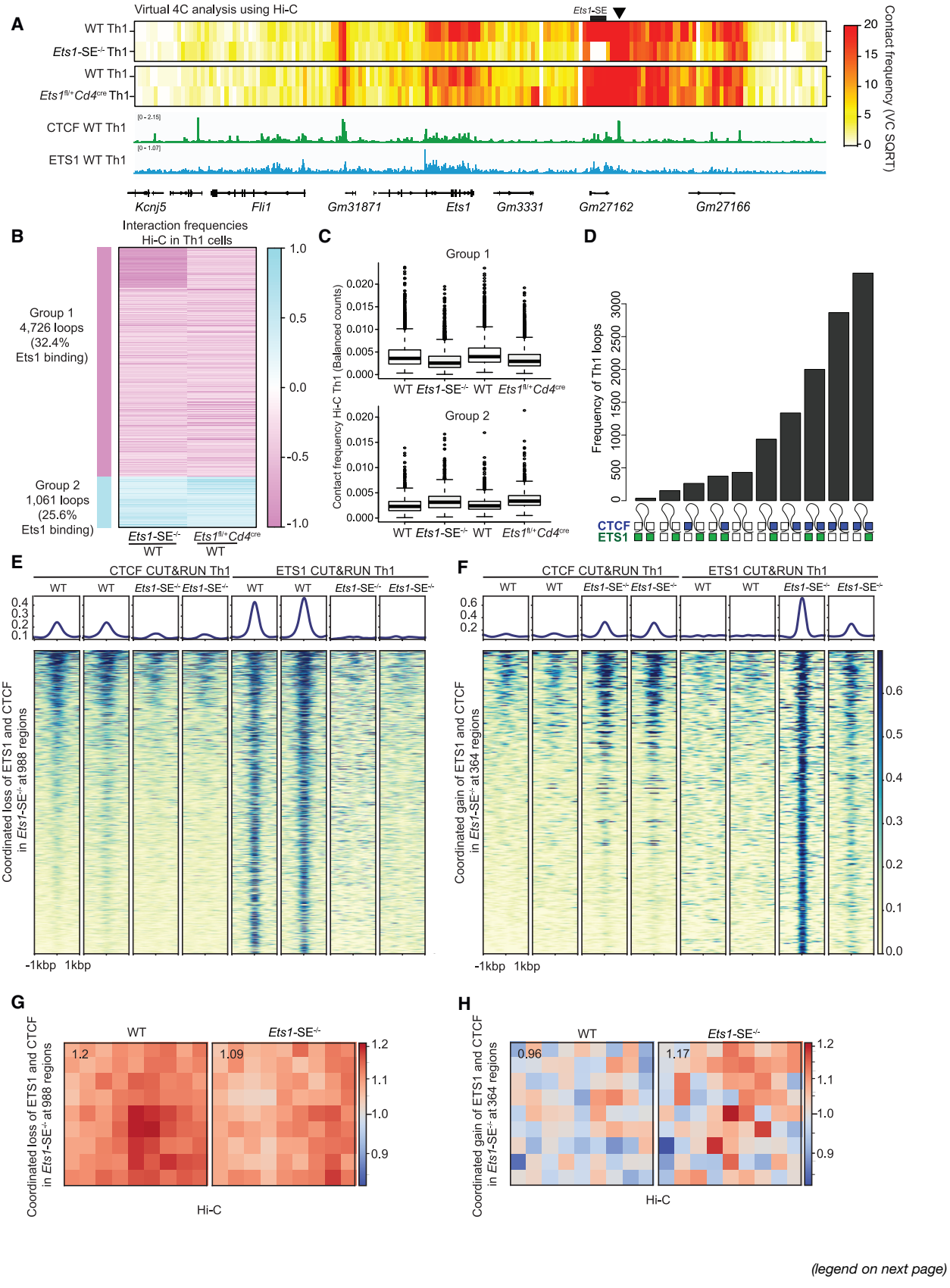

(legend on next page)

Please cite this article in press as: Chandra et al., Quantitative control of *Ets1* dosage by a multi-enhancer hub promotes Th1 cell differentiation and protects from allergic inflammation, Immunity (2023), https://doi.org/10.1016/j.immuni.2023.05.004

the functional relevance of the hyperconnectivity of this genetic hotspot in T cell biology, we generated a mouse strain wherein a noncoding regulatory element homologous to the allergy-associated polymorphic region in the human genome was deleted. T cell development was intact, but Th1 differentiation was compromised after the genetic deletion of this regulatory element. Detailed mechanistic investigation demonstrated a link between the hyperconnectivity of the *Ets1-Fli1* locus, *Ets1* expression, CTCF recruitment, and long-range interactions required for the Th1 gene expression program. Complete ablation of *Ets1* can lead to changes in CTCF recruitment,[55] and our findings further demonstrate the sensitivity of genome organization to the *Ets1* expression level as a mechanism for predisposition to immune-mediated diseases. The graded expression of interferon regulatory factor-4 (IRF-4) coordinates isotype switching with plasma cell differentiation.[58] We speculate that IRF-4 and other transcription factors may follow a similar dose-dependent mechanism and reorganize the genome by interacting with CTCF at specific genome regions.

Completion of the Human Genome Project has accelerated research on the genetic basis of Mendelian traits. In most cases, the rare single-gene disorders masquerade a multifactorial trait in their clinical phenotype,[59] but detailed clinical examination has guided to one gene responsible for the disease in those particular families. Thus, the genetic ablation of an individual gene in rodents became a powerful tool to dissect the molecular processes of such monogenic diseases. Despite the success of genetic strategies in Mendelian traits, human genetics has been less successful in dissecting complex conditions which are in fact more commonly found across populations. Unlike Mendelian traits that can be modeled as genetic deletions, complex traits might be caused by single-nucleotide variants disrupting transcriptional enhancers. Here, we present a mouse model, which was inspired by the mathematical analysis of genome organization data, reporting how noncoding elements can control the precise dosage of a key transcription factor through the formation of a multi-enhancer hub. It is worth mentioning that the heterozygous alleles of transcription factors such as HNF1A[60] or FoxA2[61] can impact target genes, leading to developmental defects. Our findings highlight dosage control through regulatory elements of the transcription factor gene, not the coding region of the transcription factor gene itself. Considering that individuals carrying risk factors for genetic predispositions to common diseases are far from genetic deletion models, we reason that comprehensive strategies following the integrative approaches used in this study can shed light on molecular mechanisms through which single-nucleotide variants can affect the gene expression programs sometimes in subtle ways, which can lead to substantial clinical phenotypes.

Limitations of the study

We are limited in oligopaint experiments to select three genomic loci, but we need to map the entire chromatin region forming a hub to better understand the dynamics of multi-enhancer interactions at the single-allele resolution. Combining RNA FISH and chromatin tracing experiments such as the optical reconstruction of chromatin architecture (ORCA)[62] can enable the investigation of gene dosage and chromatin conformation across individual alleles.

STAR★METHODS

Detailed methods are provided in the online version of this paper and include the following:

- KEY RESOURCES TABLE
- RESOURCE AVAILABILITY
  - Lead contact
  - Materials availability
  - Data and code availability
- EXPERIMENTAL MODEL AND SUBJECT DETAILS
  - Mice
- METHOD DETAILS
  - Tissue and cell Preparation
  - $CD4^+$ T cell isolation and polarization
  - ETS-1 retroviral transduction experiments
  - $CD4^+$ T cell transduction
  - Antibodies, Flow cytometry, and cell sorting
  - Flow Cytometry on *in vitro* polarized cells
  - Genomics and sequencing experiments

Figure 6. *Ets1* level controls the 3D genome topology of Th1 cells in a CTCF-dependent manner

(A) Heatmap of contact frequencies from virtual 4C analysis of Hi-C data generated from wild-type, *Ets1*-SE$^{-/-}$, and *Ets1*$^{fl/+}$*Cd4*^{cre} Th1 cells, using the immediate downstream locus of *Ets1*-SE as the 4C-anchor (chr9:32,940,001–32,945,000) (marked with black arrow). The genome browser view of the corresponding locus is shown along with CTCF and ETS1 binding tracks generated from CUT&RUN on wild-type Th1 cells.

(B) Heatmap showing $\log_2$ fold change in interaction frequencies from Hi-C in *Ets1*-SE$^{-/-}$ and *Ets1*$^{fl/+}$*Cd4*^{cre} Th1 cells, compared with their respective matched wild-type controls. Group 1 which includes 4,726 loops demonstrates weaker interactions in *Ets1*-SE$^{-/-}$ and *Ets1*$^{fl/+}$*Cd4*^{cre} Th1 cells, compared with their respective matched wild-type controls. Group 2 which includes 1,061 loops demonstrates stronger interactions in *Ets1*-SE$^{-/-}$ and *Ets1*$^{fl/+}$*Cd4*^{cre} Th1 cells, compared with their respective matched wild-type controls. The percentage of loops with ETS1 binding based on CUT&RUN in wild-type Th1 cells is also provided. Each row represents an individual interaction or a loop.

(C) Boxplot showing average interaction frequencies from Hi-C in *Ets1*-SE$^{-/-}$ and *Ets1*$^{fl/+}$*Cd4*^{cre} Th1 cells, and their respective matched wild-type controls, using group 1 and group 2 loops.

(D) UpSet plot demonstrates the number of Th1-associated loops with different binding patterns of CTCF and ETS1 across two loop anchors. A filled square represents bound, and an open square represents no binding. Blue and green squares represent CTCF and ETS1 binding, respectively. Bedtools intersect was used to define overlapping peaks with loop anchors detected in Th1 cells.

(E and F) Heatmap demonstrates CTCF and ETS1 occupancy levels at genome regions where both proteins are lost (E) and gained (F) in *Ets1*-SE$^{-/-}$ compared with wild-type Th1 cells. DESeq2 was used to define co-bound regions by ETS1 and CTCF measured by CUT&RUN with differential occupancy between wild-type and *Ets1*-SE$^{-/-}$ Th1 cells using $p < 0.05$ and $|\log FC| > 0.5$.

(G and H) Loop pileups of long-range interactions anchored at genomic regions described in (E) and (F) with lost (G) and gained (H) occupancy generated by coolpuppy. Hi-C data in wild-type and *Ets1*-SE$^{-/-}$ Th1 cells were used. The number in the top left corner represents the average intensity in a 3 × 3 box at the center.

- Oligopaint FISH probe generation
- Oligopaint FISH hybridization
- scRNA- and scATAC-seq library generation
- Genomics Data Analysis
- Hi-C data analysis
- Integration of CUT&RUN data with 3D loop analysis
- scRNA- and scATAC-seq data preprocessing and quality control
- Oligopaint FISH imaging and analysis
- Representative Image processing
- Ets1$^{+/-}$ mice data analysis
- ChIP-Atlas
- Allergy-associated SNPs enrichment

SUPPLEMENTAL INFORMATION

Supplemental information can be found online at https://doi.org/10.1016/j.immuni.2023.05.004.

ACKNOWLEDGMENTS

We thank helpful discussions with Atishay Jay and other members of the Vahedi lab in addition to Babak Faryabi, Yeqiao Zhou, Kenneth Zaret, Raj Jain, Sara Cherry, Arjun Raj, and E. John Wherry. We thank Behdad Afzali for sharing their optimized CUT&RUN protocol. We also thank the CRISPR-Cas9 Mouse Targeting Core and Transgenic & Chimeric Mouse Facility for generating the knockout mouse strains. The work in this manuscript was supported by the Burroughs Welcome Fund, the Chang Zuckerberg Initiative Award, and the NIH grant R01AI168240 (J.H.-M. and G.V.); W.W. Smith Charitable Trust, the Sloan Foundation, and the NIH grants UC4 DK112217, U01 DK112217, R01 HL145754, U01 DK127768, and U01 DA052715 (G.V.); the PEW Charitable Trust and the NIH grant R01 HL136572 (J. H-M.); and the NIH grant R01 AI106352 (B.L.K.).

AUTHOR CONTRIBUTIONS

A.C. performed *in vitro* CD4 T helper polarization experiments and all genomics-sequencing experiments with help from N.G. S.Y. performed computational analysis for genomics experiments. M.F.M. performed *in vitro* and *in vivo* phenotyping experiments in mice. E.K.F. and A.C. performed DNA FISH experiments. M.F. designed original oligopaint probes. A.C., S.Y., and E.K.F. analyzed DNA FISH data. M.A. performed multiome experiments. I.J. maintained the mouse colony. K.P. curated allergy-associated variants. L.J. generated *Ets1*-SE mouse strain. B.L.K. provided *Ets1* heterozygous cells. G.V. analyzed Mutliome data. G.V. and J.H.-M. conceptualized and supervised the project, wrote the manuscript, revised it with comments from all authors, and acquired funding.

DECLARATION OF INTERESTS

The authors declare no competing interests.

INCLUSION AND DIVERSITY

We support inclusive, diverse, and equitable conduct of research.

Received: October 22, 2022
Revised: May 6, 2023
Accepted: May 8, 2023
Published: May 31, 2023

REFERENCES

1. Iwasaki, A., and Medzhitov, R. (2015). Control of adaptive immunity by the innate immune system. Nat. Immunol. *16*, 343–353. https://doi.org/10.1038/ni.3123.
2. Johnson, J.L., Georgakilas, G., Petrovic, J., Kurachi, M., Cai, S., Harly, C., Pear, W.S., Bhandoola, A., Wherry, E.J., and Vahedi, G. (2018). Lineage-determining transcription factor TCF-1 initiates the epigenetic identity of T cells. Immunity *48*, 243–257.e10. https://doi.org/10.1016/j.immuni.2018.01.012.
3. Boller, S., Ramamoorthy, S., Akbas, D., Nechanitzky, R., Burger, L., Murr, R., Schübeler, D., and Grosschedl, R. (2016). Pioneering activity of the C-terminal domain of EBF1 shapes the chromatin landscape for B cell programming. Immunity *44*, 527–541. https://doi.org/10.1016/j.immuni.2016.02.021.
4. Emmanuel, A.O., Arnovitz, S., Haghi, L., Mathur, P.S., Mondal, S., Quandt, J., Okoreeh, M.K., Maienschein-Cline, M., Khazaie, K., Dose, M., et al. (2018). TCF-1 and HEB cooperate to establish the epigenetic and transcription profiles of CD4(+)CD8(+) thymocytes. Nat. Immunol. *19*, 1366–1378. https://doi.org/10.1038/s41590-018-0254-4.
5. Vahedi, G., Takahashi, H., Nakayamada, S., Sun, H.W., Sartorelli, V., Kanno, Y., and O'Shea, J.J. (2012). STATs shape the active enhancer landscape of T cell populations. Cell *151*, 981–993. https://doi.org/10.1016/j.cell.2012.09.044.
6. Ciofani, M., Madar, A., Galan, C., Sellars, M., Mace, K., Pauli, F., Agarwal, A., Huang, W., Parkhurst, C.N., Muratet, M., et al. (2012). A validated regulatory network for th17 cell specification. Cell *151*, 289–303. https://doi.org/10.1016/j.cell.2012.09.016.
7. Roy, R., Ramamoorthy, S., Shapiro, B.D., Kaileh, M., Hernandez, D., Sarantopoulou, D., Arepalli, S., Boller, Sr., Singh, A., Bektas, A., et al. (2022). DNA methylation signatures reveal that distinct combinations of transcription factors specify human immune cell epigenetic identity. Immunity *55*, 1135. https://doi.org/10.1016/j.immuni.2022.05.006.
8. Uyehara, C.M., and Apostolou, E. (2023). 3D enhancer-promoter interactions and multi-connected hubs: organizational principles and functional roles. Cell Rep. 112068. https://doi.org/10.1016/j.celrep.2023.112068.
9. Wang, W., Chandra, A., Goldman, N., Yoon, S., Ferrari, E.K., Nguyen, S.C., Joyce, E.F., and Vahedi, G. (2022). TCF-1 promotes chromatin interactions across topologically associating domains in T cell progenitors. Nat. Immunol. *23*, 1052–1062.
10. Johanson, T.M., Lun, A.T.L., Coughlan, H.D., Tan, T., Smyth, G.K., Nutt, S.L., and Allan, R.S. (2018). Transcription-factor-mediated supervision of global genome architecture maintains B cell identity. Nat. Immunol. *19*, 1257–1264. https://doi.org/10.1038/s41590-018-0234-8.
11. Shan, Q., Zhu, S., Chen, X., Liu, J., Yuan, S., Li, X., Peng, W., and Xue, H.H. (2022). Tcf1-CTCF cooperativity shapes genomic architecture to promote CD8(+) T cell homeostasis. Nat. Immunol. *23*, 1222–1235. https://doi.org/10.1038/s41590-022-01263-6.
12. Zhou, Y., Petrovic, J., Zhao, J., Zhang, W., Bigdeli, A., Zhang, Z., Berger, S.L., Pear, W.S., and Faryabi, R.B. (2022). EBF1 nuclear repositioning instructs chromatin refolding to promote therapy resistance in T leukemic cells. Mol. Cell *82*, 1003–1020.e15. https://doi.org/10.1016/j.molcel.2022.01.015.
13. Phanstiel, D.H., Van Bortle, K., Spacek, D., Hess, G.T., Shamim, M.S., Machol, I., Love, M.I., Aiden, E.L., Bassik, M.C., and Snyder, M.P. (2017). Static and dynamic DNA loops form AP-1-bound activation hubs during macrophage development. Mol. Cell *67*, 1037–1048.e6. https://doi.org/10.1016/j.molcel.2017.08.006.
14. Lim, B., and Levine, M.S. (2021). Enhancer-promoter communication: hubs or loops? Curr. Opin. Genet. Dev. *67*, 5–9. https://doi.org/10.1016/j.gde.2020.10.001.
15. Jiang, T., Raviram, R., Snetkova, V., Rocha, P.P., Proudhon, C., Badri, S., Bonneau, R., Skok, J.A., and Kluger, Y. (2016). Identification of multi-loci hubs from 4C-seq demonstrates the functional importance of simultaneous interactions. Nucleic Acids Res. *44*, 8714–8725. https://doi.org/10.1093/nar/gkw568.
16. Tsai, A., Alves, M.R., and Crocker, J. (2019). Multi-enhancer transcriptional hubs confer phenotypic robustness. eLife *8*. https://doi.org/10.7554/eLife.45325.

17. Allahyar, A., Vermeulen, C., Bouwman, B.A.M., Krijger, P.H.L., Verstegen, M.J.A.M., Geeven, G., van Kranenburg, M., Pieterse, M., Straver, R., Haarhuis, J.H.I., et al. (2018). Enhancer hubs and loop collisions identified from single-allele topologies. Nat. Genet. *50*, 1151–1160. https://doi.org/10.1038/s41588-018-0161-5.

18. Monahan, K., Schieren, I., Cheung, J., Mumbey-Wafula, A., Monuki, E.S., and Lomvardas, S. (2017). Cooperative interactions enable singular olfactory receptor expression in mouse olfactory neurons. eLife *6*. https://doi.org/10.7554/eLife.28620.

19. Madsen, J.G.S., Madsen, M.S., Rauch, A., Traynor, S., Van Hauwaert, E.L., Haakonsson, A.K., Javierre, B.M., Hyldahl, M., Fraser, P., and Mandrup, S. (2020). Highly interconnected enhancer communities control lineage-determining genes in human mesenchymal stem cells. Nat. Genet. *52*, 1227–1238. https://doi.org/10.1038/s41588-020-0709-z.

20. Levo, M., Raimundo, J., Bing, X.Y., Sisco, Z., Batut, P.J., Ryabichko, S., Gregor, T., and Levine, M.S. (2022). Transcriptional coupling of distant regulatory genes in living embryos. Nature *605*, 754–760. https://doi.org/10.1038/s41586-022-04680-7.

21. Petrovic, J., Zhou, Y., Fasolino, M., Goldman, N., Schwartz, G.W., Mumbach, M.R., Nguyen, S.C., Rome, K.S., Sela, Y., Zapataro, Z., et al. (2019). Oncogenic Notch promotes long-range regulatory interactions within hyperconnected 3D cliques. Mol. Cell *73*, 1174–1190.e12. https://doi.org/10.1016/j.molcel.2019.01.006.

22. Fasolino, M., Goldman, N., Wang, W., Cattau, B., Zhou, Y., Petrovic, J., Link, V.M., Cote, A., Chandra, A., Silverman, M., et al. (2020). Genetic variation in Type 1 diabetes reconfigures the 3D chromatin organization of T cells and alters gene expression. Immunity *52*, 257–274.e11. https://doi.org/10.1016/j.immuni.2020.01.003.

23. Link, V.M., Duttke, S.H., Chun, H.B., Holtman, I.R., Westin, E., Hoeksema, M.A., Abe, Y., Skola, D., Romanoski, C.E., Tao, J., et al. (2018). Analysis of genetically diverse macrophages reveals local and domain-wide mechanisms that control transcription factor binding and function. Cell *173*, 1796–1809.e17. https://doi.org/10.1016/j.cell.2018.04.018.

24. Beagrie, R.A., Scialdone, A., Schueler, M., Kraemer, D.C., Chotalia, M., Xie, S.Q., Barbieri, M., de Santiago, I., Lavitas, L.M., Branco, M.R., et al. (2017). Complex multi-enhancer contacts captured by genome architecture mapping. Nature *543*, 519–524. https://doi.org/10.1038/nature21411.

25. Boudaoud, I., Fournier, É., Baguette, A., Vallée, M., Lamaze, F.C., Droit, A., and Bilodeau, S. (2017). Connected gene communities underlie transcriptional changes in Cornelia de Lange syndrome. Genetics *207*, 139–151. https://doi.org/10.1534/genetics.117.202291.

26. Yoon, S., Chandra, A., and Vahedi, G. (2022). Stripenn detects architectural stripes from chromatin conformation data using computer vision. Nat. Commun. *13*, 1602. https://doi.org/10.1038/s41467-022-29258-9.

27. Vian, L., Pękowska, A., Rao, S.S.P., Kieffer-Kwon, K.R., Jung, S., Baranello, L., Huang, S.C., El Khattabi, L., Dose, M., Pruett, N., et al. (2018). The energetics and physiological impact of cohesin extrusion. Cell *173*, 1165–1178.e20. https://doi.org/10.1016/j.cell.2018.03.072.

28. Di Giammartino, D.C., Kloetgen, A., Polyzos, A., Liu, Y., Kim, D., Murphy, D., Abuhashem, A., Cavaliere, P., Aronson, B., Shah, V., et al. (2019). KLF4 is involved in the organization and regulation of pluripotency-associated three-dimensional enhancer networks. Nat. Cell Biol. *21*, 1179–1190. https://doi.org/10.1038/s41556-019-0390-6.

29. Zelenka, T., Klonizakis, A., Tsoukatou, D., Papamatheakis, D.A., Franzenburg, S., Tzerpos, P., Tzonevrakis, I.R., Papadogkonas, G., Kapsetaki, M., Nikolaou, C., et al. (2022). The 3D enhancer network of the developing T cell genome is shaped by SATB1. Nat. Commun. *13*. 6954. https://doi.org/10.1038/s41467-022-34345-y.

30. Song, M., Pebworth, M.P., Yang, X., Abnousi, A., Fan, C., Wen, J., Rosen, J.D., Choudhary, M.N.K., Cui, X., Jones, I.R., et al. (2020). Cell-type-specific 3D epigenomes in the developing human cortex. Nature *587*, 644–649. https://doi.org/10.1038/s41586-020-2825-4.

31. Vangala, P., Murphy, R., Quinodoz, S.A., Gellatly, K., McDonel, P., Guttman, M., and Garber, M. (2020). High-resolution mapping of multiway enhancer-promoter interactions regulating pathogen detection. Mol. Cell *80*, 359–373.e8. https://doi.org/10.1016/j.molcel.2020.09.005.

32. Hinds, D.A., McMahon, G., Kiefer, A.K., Do, C.B., Eriksson, N., Evans, D.M., St Pourcain, B., Ring, S.M., Mountain, J.L., Francke, U., et al. (2013). A genome-wide association meta-analysis of self-reported allergy identifies shared and allergy-specific susceptibility loci. Nat. Genet. *45*, 907–911. https://doi.org/10.1038/ng.2686.

33. Paternoster, L., Standl, M., Waage, J., Baurecht, H., Hotze, M., Strachan, D.P., Curtin, J.A., Bønnelykke, K., Tian, C., Takahashi, A., et al. (2015). Multi-ancestry genome-wide association study of 21,000 cases and 95,000 controls identifies new risk loci for atopic dermatitis. Nat. Genet. *47*, 1449–1456. https://doi.org/10.1038/ng.3424.

34. O'Shea, J.J., and Paul, W.E. (2010). Mechanisms underlying lineage commitment and plasticity of helper CD4 + T cells. Science *327*, 1098–1102. https://doi.org/10.1126/science.1178334.

35. Ouyang, W., Ranganath, S.H., Weindel, K., Bhattacharya, D., Murphy, T.L., Sha, W.C., and Murphy, K.M. (1998). Inhibition of Th1 development mediated by GATA-3 through an IL-4-independent mechanism. Immunity *9*, 745–755. https://doi.org/10.1016/s1074-7613(00)80671-8.

36. Kanhere, A., Hertweck, A., Bhatia, U., Gökmen, M.R., Perucha, E., Jackson, I., Lord, G.M., and Jenner, R.G. (2012). T-bet and GATA3 orchestrate Th1 and Th2 differentiation through lineage-specific targeting of distal regulatory elements. Nat. Commun. *3*, 1268. https://doi.org/10.1038/ncomms2260.

37. Fang, R., Yu, M., Li, G., Chee, S., Liu, T., Schmitt, A.D., and Ren, B. (2016). Mapping of long-range chromatin interactions by proximity ligation-assisted ChIP-seq. Cell Res. *26*, 1345–1348. https://doi.org/10.1038/cr.2016.137.

38. Mumbach, M.R., Rubin, A.J., Flynn, R.A., Dai, C., Khavari, P.A., Greenleaf, W.J., and Chang, H.Y. (2016). HiChIP: efficient and sensitive analysis of protein-directed genome architecture. Nat. Methods *13*, 919–922. https://doi.org/10.1038/nmeth.3999.

39. Vahedi, G., Kanno, Y., Furumoto, Y., Jiang, K., Parker, S.C., Erdos, M.R., Davis, S.R., Roychoudhuri, R., Restifo, N.P., Gadina, M., et al. (2015). Super-enhancers delineate disease-associated regulatory nodes in T cells. Nature *520*, 558–562. https://doi.org/10.1038/nature14154.

40. Whyte, W.A., Orlando, D.A., Hnisz, D., Abraham, B.J., Lin, C.Y., Kagey, M.H., Rahl, P.B., Lee, T.I., and Young, R.A. (2013). Master transcription factors and mediator establish super-enhancers at key cell identity genes. Cell *153*, 307–319. https://doi.org/10.1016/j.cell.2013.03.035.

41. Zhou, Y., Zhou, B., Pache, L., Chang, M., Khodabakhshi, A.H., Tanaseichuk, O., Benner, C., and Chanda, S.K. (2019). Metascape provides a biologist-oriented resource for the analysis of systems-level datasets. Nat. Commun. *10*. 1523. https://doi.org/10.1038/s41467-019-09234-6.

42. Beliveau, B.J., Joyce, E.F., Apostolopoulos, N., Yilmaz, F., Fonseka, C.Y., McCole, R.B., Chang, Y., Li, J.B., Senaratne, T.N., Williams, B.R., et al. (2012). Versatile design and synthesis platform for visualizing genomes with Oligopaint FISH probes. Proc. Natl. Acad. Sci. USA *109*, 21301–21306. https://doi.org/10.1073/pnas.1213818110.

43. Beliveau, B.J., Boettiger, A.N., Avendaño, M.S., Jungmann, R., McCole, R.B., Joyce, E.F., Kim-Kiselak, C., Bantignies, F., Fonseka, C.Y., Erceg, J., et al. (2015). Single-molecule super-resolution imaging of chromosomes and in situ haplotype visualization using Oligopaint FISH probes. Nat. Commun. *6*, 7147. https://doi.org/10.1038/ncomms8147.

44. Li, L., Leid, M., and Rothenberg, E.V. (2010). An early T cell lineage commitment checkpoint dependent on the transcription factor Bcl11b. Science *329*, 89–93. https://doi.org/10.1126/science.1188989.

45. Isoda, T., Moore, A.J., He, Z., Chandra, V., Aida, M., Denholtz, M., Piet van Hamburg, J., Fisch, K.M., Chang, A.N., Fahl, S.P., et al. (2017). Non-coding transcription instructs chromatin folding and compartmentalization to dictate enhancer-promoter communication and T cell fate. Cell *171*, 103–119.e18. https://doi.org/10.1016/j.cell.2017.09.001.

46. Dittmer, J. (2003). The biology of the Ets1 proto-oncogene. Mol. Cancer *2*, 29. https://doi.org/10.1186/1476-4598-2-29.

47. Beliveau, B.J., Kishi, J.Y., Nir, G., Sasaki, H.M., Saka, S.K., Nguyen, S.C., Wu, C.T., and Yin, P. (2018). OligoMiner provides a rapid, flexible environment for the design of genome-scale oligonucleotide in situ hybridization probes. Proc. Natl. Acad. Sci. USA *115*. E2183–E2192. https://doi.org/10.1073/pnas.1714530115.

48. Kanno, Y., Vahedi, G., Hirahara, K., Singleton, K., and O'Shea, J.J. (2012). Transcriptional and epigenetic control of T helper cell specification: molecular mechanisms underlying commitment and plasticity. Annu. Rev. Immunol. *30*, 707–731. https://doi.org/10.1146/annurev-immunol-020711-075058.

49. Powrie, F., Leach, M.W., Mauze, S., Caddle, L.B., and Coffman, R.L. (1993). Phenotypically distinct subsets of CD4+ T cells induce or protect from chronic intestinal inflammation in C. B-17 scid mice. Int. Immunol. *5*, 1461–1471. https://doi.org/10.1093/intimm/5.11.1461.

50. Skene, P.J., and Henikoff, S. (2017). An efficient targeted nuclease strategy for high-resolution mapping of DNA binding sites. eLife *6*. https://doi.org/10.7554/eLife.21856.

51. Hao, Y., Hao, S., Andersen-Nissen, E., Mauck, W.M., 3rd, Zheng, S., Butler, A., Lee, M.J., Wilk, A.J., Darby, C., Zager, M., et al. (2021). Integrated analysis of multimodal single-cell data. Cell *184*, 3573–3587.e29. https://doi.org/10.1016/j.cell.2021.04.048.

52. Bhat, N.K., Thompson, C.B., Lindsten, T., June, C.H., Fujiwara, S., Koizumi, S., Fisher, R.J., and Papas, T.S. (1990). Reciprocal expression of human ETS1 and ETS2 genes during T-cell activation: regulatory role for the protooncogene ETS1. Proc. Natl. Acad. Sci. USA *87*, 3723–3727. https://doi.org/10.1073/pnas.87.10.3723.

53. Lieberman-Aiden, E., van Berkum, N.L., Williams, L., Imakaev, M., Ragoczy, T., Telling, A., Amit, I., Lajoie, B.R., Sabo, P.J., Dorschner, M.O., et al. (2009). Comprehensive mapping of long-range interactions reveals folding principles of the human genome. Science *326*, 289–293. https://doi.org/10.1126/science.1181369.

54. Rao, S.S., Huntley, M.H., Durand, N.C., Stamenova, E.K., Bochkov, I.D., Robinson, J.T., Sanborn, A.L., Machol, I., Omer, A.D., Lander, E.S., et al. (2014). A 3D map of the human genome at kilobase resolution reveals principles of chromatin looping. Cell *159*, 1665–1680. https://doi.org/10.1016/j.cell.2014.11.021.

55. Pham, D., Moseley, C.E., Gao, M., Savic, D., Winstead, C.J., Sun, M., Kee, B.L., Myers, R.M., Weaver, C.T., and Hatton, R.D. (2019). BATF pioneers the reorganization of chromatin in developing effector T cells via Ets1-dependent recruitment of CTCF. Cell Rep. *29*, 1203–1220.e7. https://doi.org/10.1016/j.celrep.2019.09.064.

56. Hollenhorst, P.C., McIntosh, L.P., and Graves, B.J. (2011). Genomic and biochemical insights into the specificity of ETS transcription factors. Annu. Rev. Biochem. *80*, 437–471. https://doi.org/10.1146/annurev.biochem.79.081507.103945.

57. Zhao, J.Y., Osipovich, O., Koues, O.I., Majumder, K., and Oltz, E.M. (2017). Activation of mouse Tcrb: uncoupling RUNX1 function from its cooperative binding with ETS1. J. Immunol. *199*, 1131–1141. https://doi.org/10.4049/jimmunol.1700146.

58. Sciammas, R., Shaffer, A.L., Schatz, J.H., Zhao, H., Staudt, L.M., and Singh, H. (2006). Graded expression of interferon regulatory factor-4 coordinates isotype switching with plasma cell differentiation. Immunity *25*, 225–236. https://doi.org/10.1016/j.immuni.2006.07.009.

59. Peltonen, L., Perola, M., Naukkarinen, J., and Palotie, A. (2006). Lessons from studying monogenic disease for common disease. Hum. Mol. Genet. *15*. R67–R74. https://doi.org/10.1093/hmg/ddl060.

60. Nkonge, K.M., Nkonge, D.K., and Nkonge, T.N. (2020). The epidemiology, molecular pathogenesis, diagnosis, and treatment of maturity-onset diabetes of the young (MODY). Clin. Diabetes Endocrinol. *6*, 20. https://doi.org/10.1186/s40842-020-00112-5.

61. Kittappa, R., Chang, W.W., Awatramani, R.B., and McKay, R.D. (2007). The foxa2 gene controls the birth and spontaneous degeneration of dopamine neurons in old age. PLoS Biol. *5*. e325. https://doi.org/10.1371/journal.pbio.0050325.

62. Mateo, L.J., Murphy, S.E., Hafner, A., Cinquini, I.S., Walker, C.A., and Boettiger, A.N. (2019). Visualizing DNA folding and RNA in embryos at single-cell resolution. Nature *568*, 49–54. https://doi.org/10.1038/s41586-019-1035-4.

63. Henao-Mejia, J., Williams, A., Rongvaux, A., Stein, J., Hughes, C., and Flavell, R.A. (2016). Generation of genetically modified mice using the CRISPR-Cas9 genome-editing system. Cold Spring Harb. Protoc. *2016*. pdb.prot090704. https://doi.org/10.1101/pdb.prot090704.

64. Laffont, S., Blanquart, E., Savignac, M., Cénac, C., Laverny, G., Metzger, D., Girard, J.P., Belz, G.T., Pelletier, L., Seillet, C., et al. (2017). Androgen signaling negatively controls group 2 innate lymphoid cells. J. Exp. Med. *214*, 1581–1592. https://doi.org/10.1084/jem.20161807.

65. Servant, N., Varoquaux, N., Lajoie, B.R., Viara, E., Chen, C.J., Vert, J.P., Heard, E., Dekker, J., and Barillot, E. (2015). HiC-Pro: an optimized and flexible pipeline for Hi-C data processing. Genome Biol. *16*, 259. https://doi.org/10.1186/s13059-015-0831-x.

66. Roayaei Ardakany, A., Gezer, H.T., Lonardi, S., and Ay, F. (2020). Mustache: multi-scale detection of chromatin loops from Hi-C and Micro-C maps using scale-space representation. Genome Biol. *21*, 256. https://doi.org/10.1186/s13059-020-02167-0.

67. Servant, N., Varoquaux, N., Lajoie, B.R., Viara, E., Chen, C.J., Vert, J.P., Heard, E., Dekker, J., and Barillot, E. (2015). HiC-Pro: an optimized and flexible pipeline for Hi-C data processing. Genome Biol. *16*, 259.

68. Heinz, S., Benner, C., Spann, N., Bertolino, E., Lin, Y.C., Laslo, P., Cheng, J.X., Murre, C., Singh, H., and Glass, C.K. (2010). Simple combinations of lineage-determining transcription factors prime cis-regulatory elements required for macrophage and B cell identities. Mol. Cell *38*, 576–589.

69. Love, M.I., Huber, W., and Anders, S. (2014). Moderated estimation of fold change and dispersion for RNA-seq data with DESeq2. Genome Biol. *15*, 550.

70. Quinlan, A.R., and Hall, I.M. (2010). BEDTools: a flexible suite of utilities for comparing genomic features. Bioinformatics *26*, 841–842.

71. Subramanian, A., Tamayo, P., Mootha, V.K., Mukherjee, S., Ebert, B.L., Gillette, M.A., Paulovich, A., Pomeroy, S.L., Golub, T.R., Lander, E.S., et al. (2005). Gene set enrichment analysis: a knowledge-based approach for interpreting genome-wide expression profiles. Proc. Natl. Acad. Sci. U S A *102*, 15545–15550.

72. Phanstiel, D.H., Boyle, A.P., Heidari, N., and Snyder, M.P. (2015). Mango: a bias-correcting ChIA-PET analysis pipeline. Bioinformatics *31*, 3092–3098.

73. Csardi, G., and Nepusz, T. (2006). The igraph software package for complex network research. InterJournal. Complex Systems:1695.

74. Robinson, J.T., Thorvaldsdottir, H., Winckler, W., Guttman, M., Lander, E.S., Getz, G., and Mesirov, J.P. (2011). Integrative genomics viewer. Nat. Biotechnol. *29*, 24–26.

75. Phanstiel D.H. Sushi: Tools for visualizing genomics data. 2021.

76. Raj, A., van den Bogaard, P., Rifkin, S.A., van Oudenaarden, A., and Tyagi, S. (2008). Imaging individual mRNA molecules using multiple singly labeled probes. Nat. Methods *5*, 877–879.

77. Ardakany, A.R., Gezer, H.T., Lonardi, S., and Ay, F. (2020). Mustache: multi-scale detection of chromatin loops from Hi-C and Micro-C maps using scalespace representation. Genome Biol. *21*, 256.

78. Abdennur, N., Abraham, S., Fudenberg, G., Flyamer, M.I., Galitsyna, A.A., Goloborodko, A., Imakaev, M., Oksuz, B.A., and Venev, S.V. (2022). Cooltools: enabling high-resolution Hi-C analysis in Python. BioRxiv.

79. Wang, W., Chandra, A., Goldman, N., Yoon, S., Ferrari, E.K., Nguyen, S.C., Joyce, E.F., and Vahedi, G. (2022). TCF-1 promotes chromatin interactions across topologically associating domains in T cell progenitors. Nat. Immunol. *23*, 1052–1062.

80. Lawrence, M., Huber, W., Pages, H., Aboyoun, P., Carlson, M., Gentleman, R., Morgan, M.T., and Carey, V.J. (2013). Software for computing and annotating genomic ranges. PLoS Comput. Biol. *9*, e1003118.

81. Crane, E., Bian, Q., McCord, R.P., Lajoie, B.R., Wheeler, B.S., Ralston, E.J., Uzawa, S., Dekker, J., and Meyer, B.J. (2015). Condensin-driven remodelling of X chromosome topology during dosage compensation. Nature *523*, 240–244.

82. Flyamer, I.M., Illingworth, R.S., and Bickmore, W.A. (2020). Coolpup.py: versatile pile-up analysis of Hi-C data. Bioinformatics *36*, 2980–2985.

83. Stuart, T., Srivastava, A., Madad, S., Lareau, C.A., and Satija, R. (2021). Single-cell chromatin state analysis with Signac. Nat. Methods *18*, 1333–1341.

84. Li, H., Handsaker, B., Wysoker, A., Fennell, T., Ruan, J., Homer, N., Marth, G., Abecasis, G., Durbin, R., and 1000 Genome Project Data Processing Subgroup (2009). The Sequence Alignment/Map format and SAMtools. Bioinformatics *25*, 2078–2079.

85. Aguilar, S.V., Aguilar, O., Allan, R., Amir, E.D., Angeli, V., Artyomov, M.N., Asinovski, N., Astarita, J., Austen, F., Bajpai, G., et al. (2020). ImmGen at 15. Nature Immunol. *21*, 700–703.

86. Schneider, C.A., Rasband, W.S., and Eliceiri, K.W. (2012). NIH Image to ImageJ: 25 years of image analysis. Nat. Methods *9*, 671–675.

87. Zou, Z., Ohta, T., Miura, F., and Oki, S. (2022). ChIP-Atlas 2021 update: a data-mining suite for exploring epigenomic landscapes by fully integrating ChIP-seq, ATAC-seq and Bisulfite-seq data. Nucleic Acids Res. *50*, W175–W182.

Please cite this article in press as: Chandra et al., Quantitative control of *Ets1* dosage by a multi-enhancer hub promotes Th1 cell differentiation and protects from allergic inflammation, Immunity (2023), https://doi.org/10.1016/j.immuni.2023.05.004

STAR★METHODS

KEY RESOURCES TABLE

REAGENT or RESOURCE	SOURCE	IDENTIFIER
Antibodies		
Anti-mouse CD4 (Clone: RM4-5) APC	BioLegend	Cat# 100516; RRID: AB_312719
Anti-mouse CD4 (Clone: GK1.5) FITC	BioLegend	Cat# 10040; RRID: AB_312690
Anti-mouse CD4 (Clone: RM4-5) BV510	BioLegend	Cat# 100559; RRID: AB_2562608
Anti-mouse CD4 (Clone: RM4-5) BV711	BioLegend	Cat# 100549; RRID: AB_11219396
Anti-mouse CD4 (Clone: RM4-5) BV785	BioLegend	Cat# 100552; RRID: AB_2563053
Anti-mouse CD5 (Clone: 57-7.3) FITC	BioLegend	Cat# 100606; RRID: AB_312735
Anti-mouse CD8 (Clone: 53-6.7) PE-eFluor 610	Thermo Fisher Scientific	Cat# 61-0081-80; RRID: AB_2574523
Anti-mouse CD8 (Clone:53-6.7) BV785	BioLegend	Cat# 100749; RRID: AB_11218801
Anti-Mouse CD8 (Clone: 53.6-7) PerCP-Cy5.5	BioLegend	Cat# 100733; RRID: AB_2075239
Anti-mouse CD8 (Clone:53-6.7)BV711	BioLegend	Cat# 100744; RRID: AB_2562609
Anti-mouse CD11b (Clone: M1/70) AF700	BioLegend	Cat# 101222; RRID: AB_493705
Anti-mouse CD11c (Clone: N418) BV785	BioLegend	Cat# 117335; RRID: AB_11219204
Anti-mouse CD24 (Clone: M1/69) Pe/Cy7	BioLegend	Cat# 101821; RRID: AB_756047
Anti-mouse CD25 (Clone: PC61) PerCP-Cy5.5	BioLegend	Cat# 102030; RRID: AB_893288
Anti-mouse CD25 (Clone: PC61) Pacific Blue	BioLegend	Cat# 102021; RRID: AB_493642
Anti-mouse CD44 (Clone: IM7) BV785	BioLegend	Cat# 103059; RRID: AB_2571953
Anti-mouse CD44 (Clone: IM7) AF700	BioLegend	Cat# 103026; RRID: AB_493713
Anti-Mouse CD44 (Clone: IM7) PerCP-Cy5.5	BioLegend	Cat# 103035; RRID: AB_10639933
Anti-mouse CD45 (Clone: 30-F11) AF700	BioLegend	Cat# 103128; RRID: AB_493715
Anti-mouse CD45 (Clone: 30-F11) FITC	BioLegend	Cat# 103108; RRID: AB_312973
Anti-mouse CD45RB (Clone: C363-16A) PE	BioLegend	Cat# 103307; RRID: AB_313014
Anti-mouse CD62L (Clone: MEL-14) BV421	BioLegend	Cat# 104435; RRID: AB_10900082
Anti-mouse CD90.2 (Clone: 53-2.1) AF700	BioLegend	Cat# 140324; RRID: AB_2566740
Anti-rat CD90/mouse CD90.1 (Thy-1.1) (Clone: OX-7) APC/Fire™	BioLegend	Cat# 202543; RRID: AB_2650816
Anti-mouse/pig CD117 (Clone: 2B8) APC-eF780	ThermoFisher Scientific	Cat# 47-1171-82; RRID: AB_1272177
Anti-mouse CD193 (CCR3) (Clone: J07325) APC	BioLegend	Cat# 144511; RRID: AB_2565737
Anti-mouse TCRb (Clone: H57-597) FITC	BD Biosciences	Cat# 553170; RRID: AB_394682
Anti-mouse TCRb (Clone: H57-597) APC	BioLegend	Cat# 109212; RRID: AB_313435
Anti-mouse TCRb (Clone: H57-597) PE	BioLegend	Cat# 109207; RRID: AB_313430
Anti-mouse TCRb (Clone: H57-597) BB700	BD Biosciences	Cat# 745846; RRID: AB_2743291
Anti-mouse TCRb (Clone: H57-597) PE/Cy7	BioLegend	Cat# 109222; RRID: AB_893625
Anti-mouse IFNγ (Clone: XMG1.2) PerCP/Cyanine5.5	BioLegend	Cat# 505821; RRID: AB_961361
Anti-mouse IFNγ (Clone: XMG1.2) - APC	BD Biosciences	Cat# 554413; RRID: AB_398551
Anti-mouse IFNγ (Clone: XMG1.2) - AF700	BD Biosciences	Cat# 557998; RRID: AB_396979
Anti-mouse IL-13 Monoclonal Antibody (Clone: eBio13A) PE-eFluor™ 610	Thermo Fisher Scientific	Cat# 61-7133-80; RRID: AB_2574653
Anti-mouse IL-13 (Clone: eBio13A) efluor 450	Thermo Fisher Scientific	Cat# 48-7133-80; RRID: AB_11218502
Anti-mouse IL-13 (Clone: eBio13A) Alexa488 (FITC)	Thermo Fisher Scientific	Cat# 53-7133-82; RRID: AB_2016708
Anti-mouse IL-17A (Clone: TC11-18H10.1) PE	BioLegend	Cat# 506903; RRID: AB_315463
Anti-mouse IL-17A (Clone: TC11-18H10.1) BV785	BioLegend	Cat# 506928; RRID: AB_2629787
Anti-mouse IL-4 (Clone: 11B11) PE	BioLegend	Cat# 504103; RRID: AB_315317
Anti-mouse IL-5 (Clone: TRFK5) PE	ThermoFisher Scientific	Cat# 12-7052-81; RRID: AB_763588

(*Continued on next page*)

Please cite this article in press as: Chandra et al., Quantitative control of *Ets1* dosage by a multi-enhancer hub promotes Th1 cell differentiation and protects from allergic inflammation, Immunity (2023), https://doi.org/10.1016/j.immuni.2023.05.004

Continued

REAGENT or RESOURCE	SOURCE	IDENTIFIER
Anti-mouse IL-5 (Clone: TRFK5) APC	BioLegend	Cat# 504305; RRID: AB_315329
Anti-mouse Granzyme B (Clone: GB11) BV421	BioLegend	Cat# 515407; RRID: AB_2562195
T-bet Monoclonal Antibody (eBio4B10 (4B10)), PE-Cyanine7	eBioscience (Thermo Fisher Scientific)	Cat# 25-5825-80; RRID: AB_11041809
Anti-mouse/Human T-bet (Clone: 4B10) PE	eBioscience (Thermo Fisher Scientific)	Cat# 12-5825-80; RRID: AB_925762
Anti-mouse/Human T-bet (Clone: 4B10) BV711	BioLegend	Cat# 644819; RRID: AB_11218985
Anti-mouse/Human T-bet (Clone: 4B10) BV421	BioLegend	Cat# 644815; RRID: AB_10896427
Anti-mouse/Human T-bet (Clone: 4B10) PeCy7	Thermo Fisher Scientific	Cat# 25-5825-82; RRID: AB_11042699
Anti-Mouse RORγt Antibody (Clone: Q31-378) BV421	BD Biosciences	Cat# 562894; RRID: AB_2687545
Anti-mouse RORγt (Clone: B2D) PE	Thermo Fisher Scientific	Cat# 12-6981-82; RRID: AB_10807092
Anti-mouse RORγt (Clone: B2D) PE-eFluor 610	Thermo Fisher Scientific	Cat# 61-6981-80; RRID: AB_2574649
Anti-mouse Ly6G (Clone: 1A8) FITC	BioLegend	Cat# 127606; RRID: AB_1236494
Anti-mouse Eomes (Clone: Dan11mag) APC	ThermoFisher Scientific	Cat# 17-4875-82; RRID: AB_2866428
Anti-mouse GATA3 (Clone: L50-823) BV711	BD Biosciences	Cat# 565449; RRID: AB_2739242
Anti-mouse GATA3 (Clone: L50-823) PeCy7	BD Biosciences	Cat# 560405; RRID: AB_1645544
Anti-mouse FoxP3 (Clone: MF-14) BV421	BioLegend	Cat# 126410; RRID: AB_2105047
Anti-mouse FoxP3 (Clone: MF-14) PE	BioLegend	Cat# 126403; RRID: AB_1089118
Anti-mouse NK1.1 (Clone: PK136) BV711	BioLegend	Cat# 108745; RRID: AB_2563286
Anti-mouse NK1.1 (Clone: PK136) FITC	BioLegend	Cat# 108705; RRID: AB_313392
Anti-Mouse CD1d-PE (PBS57 - NIH Core)	NIH Tetramer Core Facility	Item # 14461; RRID: N/A
Anti-mouse SiglecF (Clone: S17007L) PE	BioLegend	Cat# 155505; RRID: AB_2750234
Anti-mouse Siglec-F (Clone: E50-2440) PE-CF594	BD Biosciences	Cat# 562757; RRID: AB_2687994
Anti-mouse T1/ST2 (Clone: DIH9) PeCy7	BioLegend	Cat# 145304; RRID: AB_2561915
Anti-CD3ε Armenian Hamster Monoclonal Antibody (LEAF - Clone: 145-2C11)	BioLegend	Cat# 100302; RRID: AB_312667
Anti-CD28 Syrian Hamster Monoclonal Antibody (Clone: 37.51)	BD Biosciences	Cat# 553294; RRID: AB_394763
InVivoMab anti-mouse IFNγ (Clone: XMG1.2)	Bio X Cell	Cat# BE0055; RRID: AB_1107694
InVivoMab anti-mouse IL-4 (Clone: 11B11)	Bio X Cell	Cat# BE0045; RRID: AB_1107707
Anti-CTCF	Millipore	Cat# 07-729; RRID: AB_441965
Anti-Acetyl-Histone H3 (Lys27) (D5E4)	Cell Signaling Technology	Cat# 8173; RRID: AB_10949503
Anti-Ets1 (C-20)	Santa Cruz Biotechnology	Cat# sc-350; RRID: AB_2100688
Anti-CD8 (biotin) (clone: 53-6.7)	BioLegend	Cat# 100704; RRID: AB_312743
Anti-CD19 (biotin)(clone: 6D5)	BioLegend	Cat# 115504; RRID: AB_313639
Anti-CD45R (biotin) (clone: RA3-6B2	BioLegend	Cat# 103204; RRID: AB_312989
Anti-Gr1 (biotin) (clone: RB6-8C5)	BioLegend	Cat# 108403; RRID: AB_313368
Anti-TCRg/d (biotin) (clone: GL3)	BioLegend	Cat# 118103; RRID: AB_313827
Anti-CD11c (biotin) (clone: N418)	BioLegend	Cat# 117303; RRID: AB_313772
Anti-I-A/I-E (biotin)(clone: M5)	BioLegend	Cat# 107604; RRID: AB_313319
Anti-CD25 (biotin) (clone: PC61)	BioLegend	Cat# 102003; RRID: AB_312852
Anti-NK1.1 (biotin) (clone:PK136)	BioLegend	Cat# 108703; RRID:AB_313390
Chemicals, peptides, and recombinant proteins		
Recombinant IL-2 (mouse)	BioLegend	Cat# 575402
Recombinant IL-12 (mouse)	BioLegend	Cat# 577002
Recombinant TGFb (mouse)	BioLegend	Cat# 763102
Recombinant IL-4 (mouse)	BioLegend	Cat# 574302
Recombinant IL-6 (mouse)	BioLegend	Cat# 575702

(*Continued on next page*)

Please cite this article in press as: Chandra et al., Quantitative control of *Ets1* dosage by a multi-enhancer hub promotes Th1 cell differentiation and protects from allergic inflammation, Immunity (2023), https://doi.org/10.1016/j.immuni.2023.05.004

Continued

REAGENT or RESOURCE	SOURCE	IDENTIFIER
Viability Dye LIVE/DEAD™ Fixable Aqua Dead Cell Stain Kit	ThermoFisher Scientific	Cat# L34957
Fixable Viability Dye eFluor™ 506	ThermoFisher Scientific	Cat# 65-0866-14
Fixable Viability Dye eFluor™ 520	ThermoFisher Scientific	Cat# 65-0867-14
Fixable Viability Dye eFluor™ 780	ThermoFisher Scientific	Cat# 50-112-9035
CellTrace™ Violet Cell Proliferation Kit, for flow cytometry	ThermoFisher Scientific	Cat# C34557
HDM extracts (Dermatophagoides pteronyssinus extracts)	Fischer Scientific (Greer Laboratories)	Cat# NC9756554 (lot: 361863, 385930, 387032)
Phorbol 12-myristate 13-acetate (PMA)	Sigma- Aldrich	Cat# P8139-1MG
Ionomycin calcium salt from Streptomyces conglobatus	Sigma- Aldrich	Cat# I0634-1MG
GolgiPlug Protein Transport Inhibitor	BD Biosciences	Cat# 555029
RPMI 1640 medium	Invitrogen	Cat# 11875085
Fetal Bovine Serum	Sigma- Aldrich	Cat# F2442
GemCell™ - Fetal Bovine Serum	Gemini Bio	Cat# 100-500, Lot# A03HOOK
2-bMercaptoethanol	Sigma	Cat# M6250-10ML
ACK Lysing Buffer	ThermoFisher Scientific	Cat# A1049201
Deoxyribonuclease I from bovine pancreas	Sigma-Aldrich	Cat# D5025
Collagenase D	Roche	Cat# 11088866001
Dispase (5U/ml)	STEMCELL Technologies	Cat# 07913
HEPES	ThermoFisher	Cat#15630080
Non-Essential Amino Acids	ThermoFisher	Cat#11140050
Penicillin-Streptomycin	ThermoFisher	Cat# 15140122
Sodium Pyruvate	ThermoFisher	Cat# 11360070
L-Glutamine (200 mM)	ThermoFisher	Cat# 25030081
Percoll® Density Gradient Media	VWR	Cat# 17-0891-01
Formaldehyde solution 16%	Thermo	Cat# PI28908
cOmplete™, EDTA-free Protease Inhibitor Cocktail	Roche	Cat# 11873580001
Qubit dsDNA HS Assay Kit	Invitrogen	Cat# Q32851
Phusion PCR Master Mix	NEB	Cat# M0531
Nextera XT Index Kit	Illumina	Cat# FC-131-1001
SPRIselect	Beckman Coulter	Cat# B2331
Polybrene	Sigma	Cat# H9268
Lipofectamine 3000	Thermo	Cat# L3000008
Chloroquine	Sigma	Cat# C6628-25G
Secondary Oligopaint probe: /5Alex647N/ TGATCGACCACGGCCAAGAC GGAGAG CGTGTG/ 3AlexF647N/	https://www.pnas.org/doi/full/10.1073/pnas.1714530115	N/A
Secondary Oligopaint probe: /5ATTO565N/ ACACN/ACCTTGCACGTCGTGGACCTCC TGCGCTA/ 3ATTO565N/	https://www.pnas.org/doi/full/10.1073/pnas.1714530115	N/A
Secondary Oligopaint probe: /5Alex488N/ CACAN/ACGCTCTTCCGTTCTATGCGAC GTCGGTG/ 3AlexF488N/	https://www.pnas.org/doi/full/10.1073/pnas.1714530115	N/A
Polysine microscope slides	Thermo Scientific	Cat# P4981-001
Silicone isolators	Electron Microscopy Sciences	Cat# 70339-05
Ethanol	Decon Laboratories	Cat# 2716
Dimethylformamide	Sigma-Aldrich	Cat# D4551
Polyvinylsulfonic acid (PVSA)	Sigma Aldrich	Cat# 278424

(*Continued on next page*)

Please cite this article in press as: Chandra et al., Quantitative control of *Ets1* dosage by a multi-enhancer hub promotes Th1 cell differentiation and protects from allergic inflammation, Immunity (2023), https://doi.org/10.1016/j.immuni.2023.05.004

Continued

REAGENT or RESOURCE	SOURCE	IDENTIFIER
Coverslips	Fisher Scientific	Cat# 12-548-5M
Nowrinkle rubber cement	Elmer's	N/A
Slowfade Gold Antifade Reagent	Invitrogen by Thermo Fisher Scientific	Cat# S36936
Dries instantly top coat	Sally Hansen's	Cat# 45114
Fixation/Permeabilization Solution Kit	BD Biosciences	Cat#554714
Foxp3/ Transcription Factor Staining Buffer Set	Thermo	Cat# 00-5523-00
Critical commercial assays		
CUTANA™ ChIC/CUT&RUN Kit	EpiCypher	Cat# 14-1048
Tn5 Transposase	Illumina	Cat# FC-121-1030
SMARTer Stranded Total RNA-Seq Kit – Pico Input Mammalian kit	Takara	Cat# 635006
NEBNext Ultra II DNA Library Prep Kit for Illumina	NEB	Cat# E7645S
D1000 ScreenTape	Agilent	Cat# 5067-5582
D1000 Reagents	Agilent	Cat# 5067-5583
High Sensitivity D1000 ScreenTape	Agilent	Cat# 5067-5584
High Sensitivity D1000 Reagents	Agilent	Cat# 5067-5585
Genomic DNA ScreenTape	Agilent	Cat# 5067-5365
Genomic DNA Reagents	Agilent	Cat# 5067-5366
RNA ScreenTape	Agilent	Cat# 5067-5576
RNA ScreenTape Ladder	Agilent	Cat# 5067-5578
RNA ScreenTape Sample Buffer	Agilent	Cat# 5067-5577
Arima HiC kit	Arima Genomics	N/A
Accel-NGS 2S Plus DNA Library Kit	Swift Biosciences	Cat# 21024
MinElute Reaction Cleanup Kit	QIAGEN	Cat# 28204
QIAQuick PCR Purification Kit	QIAGEN	Cat# 28104
RNeasy Plus Micro Kit	QIAGEN	Cat# 74034
EasySep™ Mouse Naïve CD4+ T Cell Isolation Kit	StemCell	Cat# 19765
Chromium Next GEM Single Cell Multiome ATAC + Gene Expression Reagent Bundle, 16 rxns	10X Genomics	PN-1000283
Chromium Next GEM Chip J Single Cell Kit, 48 rxns	10X Genomics	PN-1000234
Single Index Kit N Set A, 96 rxns	10X Genomics	PN-1000212
Dual Index Kit TT Set A, 96 rxns	10X Genomics	PN-1000215
Deposited data		
HiC, CUT&RUN, ATAC-seq and RNA-seq	This study	GEO: GSE211178
Experimental models: Organisms/strains		
Mouse: C57BL/6J	Jackson Laboratories	RRID:IMSR_JAX:000664
Mouse: C57BL/6J-Ets1-SE$^{-/-}$	This study	N/A
Mouse: CD4-cre (B6.Cg-Tg(Cd4-cre) 1Cwi/BfluJ)	The Jackson Laboratory	Cat#022071; RRID:IMSR_JAX:022071
Mouse: Ets1$^{fl/fl}$	Gift from Barbara L. Kee	N/A
Mouse: Rag1$^{-/-}$mice (B6.129S7-Rag1tm1Mom/J)	Jackson Laboratories	Strain #:002216, RRID:IMSR_JAX:002216
Recombinant DNA		
Plasmid: MSCV-IRES-Thy1.1 DEST	Addgene	Cat# 17442
Plasmid: pCL-Eco	Naviaux et al., 1996	N/A
Software and algorithms		
R 4.1.1	R Core Team[60]	https://www.R-project.org/
Python 3.8	Van Rossum and Drake[61]	https://peps.python.org/pep-0569/

(*Continued on next page*)

Please cite this article in press as: Chandra et al., Quantitative control of *Ets1* dosage by a multi-enhancer hub promotes Th1 cell differentiation and protects from allergic inflammation, Immunity (2023), https://doi.org/10.1016/j.immuni.2023.05.004

Continued

REAGENT or RESOURCE	SOURCE	IDENTIFIER
FastQC v0.11.9	Andrews[62]	http://www.bioinformatics.babraham.ac.uk/projects/fastqc/
Trim_Galore v0.6.6	Krueger[41]	https://github.com/FelixKrueger/TrimGalore
BWA v0.7.17-r1188	Li & Durbin[43]	https://bio-bwa.sourceforge.net
Picard v2.26.7	Broad Institute[63]	http://broadinstitute.github.io/picard/
MACS2 v2.1.4	Zhang et al.[64]	https://pypi.org/project/MACS2/2.1.4/
bamCoverage v3.3.2	Ramirez et al.[65]	https://deeptools.readthedocs.io/en/develop/content/tools/bamCoverage.html
STAR v2.7.7a	Dobin et al.[66]	https://github.com/alexdobin/STAR
HiC-Pro v2.8	Servant et al.[67]	https://github.com/nservant/HiC-Pro/
Homer	Heinz et al.[68]	http://homer.ucsd.edu/homer/
DESeq2 v1.34.0	Love, Huber, and Anders[69]	https://bioconductor.org/packages/release/bioc/html/DESeq2.html
bedtools v2.30.0	Quinlan and Hall[70]	https://bedtools.readthedocs.io/en/latest/content/installation.html
GSEA v4.3.2	Subramanian et al.[71]	https://www.gsea-msigdb.org/gsea/index.jsp
Mango v1.2.0	Phanstiel et al.[72]	https://github.com/dphansti/mango
igraph v1.3.5	Csardi and Nepusz[73]	https://igraph.org
Seurat v4.3.0	Hao et al.[47]	https://satijalab.org/seurat/
Integrative Genome Browser v2.9.13	Robinson et al.[74]	https://software.broadinstitute.org/software/igv/
Cell Ranger-ARC v2.0.0		https://support.10xgenomics.com/single-cell-multiome-atac-gex/software/pipelines/latest/what-is-cell-ranger-arc
Sushi v1.32.0	Phanstiel[75]	http://bioconductor.riken.jp/packages/3.1/bioc/html/Sushi.html
RajLabImageTool v1.0	Raj et al.[76]	https://github.com/arjunrajlaboratory/rajlabimagetools
Mustache v1.2.7	Ardakany et al.[77]	https://github.com/ay-lab/mustache
Deeptools v3.5.1	Ramirez et al.[65]	https://deeptools.readthedocs.io/en/develop/
Oligominer	Beliveau et al.[44]	https://github.com/beliveau-lab/OligoMiner
Cooltools	Abdennur et al.[78]	https://github.com/open2c/cooltools
Cool_compartment.py	Wang et al.[79]	https://github.com/VahediLab/TCF13D_code/blob/master/Figure4/cool_compartment.py
GenomicRanges v1.46.1	Lawrence et al.[80]	https://bioconductor.org/packages/release/bioc/html/GenomicRanges.html
Matrix2insulation.pl	Crane et al.[81]	https://github.com/dekkerlab/cworld-dekker/commit/09dd804f8cf9f7522351b97d6b22296b75d2d7f8
Insulation2tads.pl	Crane et al.[81]	https://github.com/dekkerlab/cworld-dekker/blob/master/scripts/perl/insulation2tads.pl
Stripenn v1.1.65.15	Yoon et al.[14]	https://github.com/ysora/stripenn
Coolpup.py v0.9.5	Flyamer et al.[82]	https://github.com/open2c/coolpuppy
Signac v1.9.0	Stuart et al.[83]	https://cran.r-project.org/web/packages/Signac/
Samtools 1.11	Li et al.[84]	https://samtools.sourceforge.net
ImmGen	The Immunological Genome Project[85]	https://www.immgen.org
ImageJ	Schneider et al.[86]	https://imagej.net
ChIP-Atlas	Zou et al.[87]	https://chip-atlas.org

(*Continued on next page*)

Continued

REAGENT or RESOURCE	SOURCE	IDENTIFIER
FlowJo v10.8.2	TreeStar	https://www.flowjo.com/solutions/flowjo/downloads
GraphPad Prism 9 Version 9.5.1 (528), January 24, 2023	GraphPad Software	https://www.graphpad.com/scientific-software/prism/

RESOURCE AVAILABILITY

Lead contact

Further information and requests for resources and reagents should be directed to and will be fulfilled by the lead contact, Golnaz Vahedi (vahedi@pennmedicine.upenn.edu).

Materials availability

This study did not generate new unique reagents.

Data and code availability

The accession number for the HiC, CUT&RUN, ATAC-seq and RNA-seq reported in this study is NCBI GEO: GSE211178. All codes used for data analysis in this paper are public and listed in the key resources table. Any additional information required to reanalyze the data reported in this paper is available from the lead contact upon request.

EXPERIMENTAL MODEL AND SUBJECT DETAILS

Mice

The *Ets1*-SE$^{-/-}$ mice were generated using the CRISPR/Cas9 system as previously described.[63] The sgRNA sequences 5′ GGACGTTGTGCACCTAGGATTGG and 3' ATAAACGTCAATAATGGTATAGG were used for the generation of knockout mice and allowed the deletion of the following DNA regions referred to as *Ets1*-SE: chr9:32,928,966-32,904,069 (mm10 genome). *Ets1*-SE$^{-/-}$ mice were backcrossed onto the C57BL/6 background for at least three generations to control for potential off-target effects. *Rag1*$^{-/-}$ mice (B6.129S7-Rag1tm1Mom/J; Strain #:002216) were purchased from the Jackson Laboratory. *Ets1*$^{fl/fl}$ *Cd4*^{cre} mice were generated by Dr. Barbara Kee's laboratory at the University of Chicago by insertion of loxP sites flanking exons 7 and 8 of the *Ets1* locus. Ets1$^{fl/+}$ mice were then crossed to mice expressing the Cre recombinase under the *Cd4* promoter (*Cd4*^{cre}) to generate *Cd4*^{cre} *Ets1*$^{fl/+}$ mice. Spleens and lymph nodes (LNs) from these mice were used for *in vitro* polarization assays. All mice were bred and maintained under pathogen-free conditions at an American Association for the Accreditation of Laboratory Animal Care accredited animal facility at the University of Pennsylvania. Mice were housed in accordance with the procedures outlined in the Guide for the Care and Use of Laboratory Animals under an animal study proposal approved by an institutional Animal Care and Use Committee. All experiments were performed using 6- to 12-weeks old age and sex matched mice and using both males and females.

METHOD DETAILS

Tissue and cell Preparation

Different organs were extracted from the mice for T cell phenotyping study, including thymus, lungs, liver, spleen, lymph nodes and bone marrow. All red blood cells were lysed using ACK lysis buffer (GIBCO). Single-cell suspensions from spleen, thymus and lymph nodes were isolated by physical dissociation of tissues and filtered through a 70μm cell strainer (Falcon) in RPMI-1640 media (Invitrogen) containing 1% fetal bovine serum (FBS) (Fisher Scientific). For bone marrow cell isolation, femurs were collected and crushed using a mortar and pestle. Lungs were isolated, minced with scissors, and digested in PBS containing FBS (2%), Collagenase D (1mg/ml), DNase I (0.2mg/ml) for 35 minutes at 37°C with shaking at 200 RPM. The digested lungs were then passed through a 70μm cell strainer. Mice were perfused with 10ml PBS and then transferred to DMEM on ice. The liver was then removed from media and mechanically dissociated using a tissue grinder, then filtered through a 100μm cell strainer. To pellet hepatocytes, the digested livers were centrifuged at 20g for 5min at 4°C. Leukocytes were then purified over an 80/40% Percoll gradient.

CD4$^+$ T cell isolation and polarization

Splenocytes were isolated from mouse spleen and lymph nodes. Spleen cells were subjected to ACK lysis buffer (Gibco, Invitrogen) to remove red blood cells. Naïve CD4$^+$ T cells were enriched using negative selection beads (STEMCELL, Cat# 19765) following manufacturer's recommendations. Purity of naïve cells were assessed using flow cytometry and found to be >=90% pure. Cells were cultured in RPMI 1640 medium (Invitrogen), supplemented with 10% fetal bovine serum (Fisher Scientific), 1mM sodium pyruvate (Gibco), 1% non-essential amino acids (Gibco), 1X GlutaMAX (Gibco), 1% HEPES (Gibco), 1% penicillin-streptomycin and 0.1% 2-Mercaptoethanol (Gibco). For *in vitro* polarization, flat bottom 96-well plates were coated with 2 μg/mL of anti-CD3 (Clone: 145-2C11, BioLegend, Cat#100302) in PBS overnight at 4°C or 4 hrs at 37°C. For Th1 polarization, 0.2x10^6 naïve CD4$^+$ T cells were

cultured in presence of 10 ng/mL of recombinant IL-12 (BioLegend, Cat#577002), 1 ng/mL of recombinant IL-2 (BioLegend, Cat#575402) and 1 μg /mL of soluble anti-CD28 (Clone: 37.51, BD Biosciences, Cat# 553294) for 6 days at 37°C. Th2 polarization was induced by cultivating $0.2x10^6$ naïve $CD4^+$ T cells in complete RPMI supplemented with 10 μg /mL of anti-IFNγ (Clone: XMG1.2, BioXCell, Cat#BE0055), 50 ng/mL of recombinant IL-4 (BioLegend, Cat# 574302) and 1 μg/mL of soluble anti-CD28 for 6 days at 37°C. For Th17 polarization, $0.2x10^6$ naïve $CD4^+$ T cells were cultured in complete RPMI containing 10 μg/mL of anti-IFNγ, 10 μg/mL of anti-IL-4 (Clone: 11B11, BioXCell, Cat# BE0045), 2 ng/mL of recombinant TGFβ (BioLegend, Cat#763102), and 20 ng/mL of recombinant IL-6 (BioLegend, Cat# 575702) and 1 μg/mL of soluble anti-CD28 for 6 days at 37°C. For induced Treg (iTreg) polarization, $0.2x10^6$ naïve $CD4^+$ T cells were cultured in complete RPMI containing 10 μg/mL of anti-IFNγ (Clone: XMG1.2, BioXCell, Cat#BE0055), 10 μg/mL of anti-IL-4 (Clone: 11B11, BioXCell, Cat# BE0045), 3 ng/mL of recombinant TGFβ (BioLegend, Cat#763102), and 5 ng/mL of recombinant IL-2 (BioLegend, Cat# 575702) and 2 μg/mL of soluble anti-CD28 for 6 days at 37°C. At day 3 post stimulation, half of the medium was removed and replaced by fresh media containing 2X cytokines concentration of Th1, Th2 or Th17-related polarizing medium.

ETS-1 retroviral transduction experiments

cDNA encoding the short isoform of ETS-1 (p54) was cloned into pENTR vector and then into the destination vector MSCV-IRES-Thy1.1 DEST (Addgene: 17442) using Gateway cloning strategy (Gateway Clonase II, Invitrogen). To generate retroviral particles for Ets1-overexpression, 293T cells were purchased from ATCC. Briefly, HEK-293T cells were maintained in high glucose DMEM medium 1X with L-Glutamine (Invitrogen), supplemented with 100 U/mL penicillin and 100 mg/mL streptomycin (Gibco) with 10% FBS. Cells were maintained at low passage number (< 12), at 70-80% confluency, and were grown at 37°C and 5% CO2. Retroviral vectors were packaged in HEK 293T cells. Briefly, $4x10^6$ HEK 293T cells were plated in 5 ml media in 10 cm dishes on the day prior to transfection. During transfection, 15 μg of MSCV-Thy1.1-Ets1 plasmid was co-transfected with packaging plasmid, 15 μg of pCL-Eco, using Lipofectamine 3000 (Invitrogen). The MSCV-Thy1.1-EV (Empty vector) plasmid was also similarly transfected. The cells were returned to the incubator for 6 hours. Subsequently, the medium was changed to fresh media. Virions were collected 24 and 48 hrs after transfection, snap-frozen, and stored at -80°C for future use.

$CD4^+$ T cell transduction

Primary naïve $CD4^+$ T cells were transduced by addition of virions to culture media supplemented with polybrene (Sigma-Aldrich, cat# H9268) at 4 μg/mL final concentration, followed by centrifugation at 32°C for 1 hour at 3000 rpm. Cells were returned to incubator at 37°C for at least 4 hrs. Subsequently, the medium was changed to fresh culture media supplemented with Th1 polarizing cytokines. Transduction efficiency was checked next day and frequency of polarizing cells was checked on day 6 after transduction.

Antibodies, Flow cytometry, and cell sorting

All antibodies were diluted in FACS buffer (PBS + 2% FBS + 2mM EDTA) and used to stain single cell suspensions for 30 minutes at 4°C. First, dead cells were stained by incubation of cell suspension in Viability Dye (eFluor780, eFluor506, or Aqua) diluted in PBS for 10mins at 4°C. Then after a wash with PBS, cells were staining with surface antibodies diluted in FACS buffer (PBS + 2% FBS + 2mM EDTA) and washed with FACS buffer. Cells were then either fixed for intracellular staining using the Foxp3 staining buffer (eBioscience) or were fixed with 2% PFA. For intracellular staining, fixed cells were washed with permwash buffer (eBioscience) and incubated with intracellular antibodies diluted in permwash buffer for 30 mins or left overnight. Cells were washed with permwash buffer and resuspended in FACS buffer with the addition of 123count eBeads (ThermoFischer Scientific, ref:01-1234-42) following manufacturer's recommendations for cell counting. For cell sorting, cells were stained at a concentration of $100x10^6$ cells/ml in FACS buffer (PBS + 2% FBS + 2mM EDTA) for 30 mins at 4°C then filtered through a 70μm filter prior acquisition and sort using either a 100μm or 70μm nozzle on a BD FACS Aria II SORP under aseptic conditions. Cells were sorted in FACS buffer containing 10% of FBS.

Flow Cytometry on *in vitro* polarized cells

For flow cytometry, *in vitro* polarized cells were stimulated with PMA, Ionomycin and Golgi Plug for 4 hrs at 37C. Subsequently, they were stained with a viability dye (1:500 L/D Aqua), and extracellular stains with anti-mouse CD4-APC (1:400, clone RM4-5, BioLegend Cat#100516), anti-mouse TCRb chain-FITC (1:400, clone H57-597, BD Biosciences Cat#553170). Cell were then fixed using Foxp3/Transcription factor Staining buffer Set (eBioscience, Thermo Cat# 00-5523-00) followed by intra-cellular stains with anti-mouse IFNγ-PerCP/Cyanine5.5 (1:200, clone XMG1.2, BioLegend Cat#505821), T-bet monoclonal antibody-PE-Cyanine 7 (1:200, clone 4B10, eBioscience, Cat# 25-5825-80), anti-mouse IL-13-PE eFluor 610 (clone eBio13A, Fisher Cat# 61-7133-80), anti-GATA3 BV711 (BD Biosciences Cat# 565449), anti-mouse IL-17 PE (clone TC11-18H10.1, BioLegend, Cat# 506903), anti-mouse RORgt BV421 (BD Biosciences Cat#562894). Cells were washed and resuspended in PBS for flow cytometry. Data were collected on an LSR II running DIVA software (BD Biosciences) and were analysed using FlowJo software v10.8.1.

In vivo *House Dust Mite (HDM) extract exposure model*

HDM extracts (*Dermatophagoides pteronyssinus* extracts; Greer Laboratories lot #361863, 385930, 387032) were used to induce allergic airway inflammation, following the protocol described previously.[64] Briefly, mice were sensitized intranasally with 20 μg HDM extracts on day 0 and subsequently challenged intranasally with 10 μg/mouse per day on days 7–13. Three days after the last challenge, mice were anesthetized and used either for immune cell quantification in the lung parenchyma or *ex vivo* restimulation. For lung parenchyma experiments, lungs were isolated, minced with scissors, and digested in PBS containing FBS (2%), Collagenase

Please cite this article in press as: Chandra et al., Quantitative control of *Ets1* dosage by a multi-enhancer hub promotes Th1 cell differentiation and protects from allergic inflammation, Immunity (2023), https://doi.org/10.1016/j.immuni.2023.05.004

D (1mg/ml), DNase I (0.2mg/ml) for 35 minutes at 37°C with shaking at 200 RPM. The digested lungs were then passed through a 70μm cell strainer. Cells were resuspended in PBS then split in order to perform lung parenchyma cell infiltration or *ex vivo* restimulation. For *ex vivo* restimulation, cells were plated into round-bottom 96 well plates and stimulated in complete RPMI media containing PMA (Sigma; final concentration 100ng/mL) and Ionomycin (Sigma; final concentration 10ng/mL) and GolgiPlug (1X - BD Bioscience). Cytokines and transcription factor expression were measured by intracellular staining using the "Foxp3 staining buffer" (Ebioscience).

Induction and Evaluation of colitis

$CD4^+$ T cells were enriched from spleen and lymph node cell suspensions using a cocktail of biotinylated antibodies containing anti-CD8 (53-6.7), anti-CD19 (6D5), anti-BB20 (RA3-6B2), anti-Gr1 (RB6-8C5), anti-TCRγδ (GL3), anti-CD11c (N418), anti-I-A/I-E (M5), anti-CD25 (PC61) all purchased from Biolegend. Splenocytes were incubated for 30mins at 4°C with the previously mentioned mAbs, washed with PBS then incubated with streptavidin magnetic beads for 20mins at 4°C. Negative fraction containing CD4 T cell was then stained with Viability Dye-APC-eF780, anti-TCRβ-APC (H57-597), anti-CD4-FITC (GK1.5), anti-CD8-PerCP-Cy5.5 (53-6.7) and anti-CD45RB-PE (C363-16A) mAbs. Live, $TCR\beta^+$, $CD4^+$, $CD45RB^{high}$ colitogenic T cells were then separated by fluorescent cell sorting using a BD FACS Aria II SORP with a purity over 90%. Colitis was induced in 9- to 11-week-old $Rag1^{-/-}$ mice by retro-orbital injection of $1x10^6$ naive $CD4^+CD45RB^{high}$ from WT or *Ets1*-$SE^{-/-}$ colitogenic $CD4^+$ T cells in 100 μl of PBS. Weight loss of *Ets1*-$SE^{-/-}$ or WT-injected $Rag1^{-/-}$ was recorded every week for 6 to 7 weeks prior to mice euthanasia. Cell infiltration characterization, restimulation and macroscopic scoring was performed on week 6 to 7.

Macroscopic analysis

Macroscopic colonic tissue damage was evaluated by the Comparative Pathology Core (CPC) at the Veterinary school of the University of Pennsylvania using a scale described in Figure 3E. Colonic tissue specimens were excised 2 cm proximal to the cecum and immediately transferred into 10% formaldehyde to be embedded in paraffin. Colonic sections were then stained with hematoxylin and eosin by the Comparative Pathology Core (CPC) at the Veterinary school of the University of Pennsylvania. Each slide was scored (blind readings) by a single pathologist. Colon length was measured using a ruler right after mice euthanasia (Figure S2A)

Colon Lamina propria (cLP) harvest digestion and cell infiltration phenotyping

Colons were excised and fat was removed using forceps, unrolled, and measured using a ruler. Colons were flushed with cold PBS to remove feces then were opened lengthwise and tissues were shaken in a petri dish containing cold PBS to remove any remaining feces. Colons were washed 2 times 10mins at 180 RPM and 37°C in PBS containing FBS (2%), HEPES (20mM) and EDTA (10mM). Colons were thoroughly washed 2 times with ice cold PBS and minced into 1 cm pieces using scissors. The minced colons were then digested PBS containing FBS (2%), HEPES (20mM), Collagenase D (1mg/ml), DNAse I (0.2mg/mL), and Dispase (0.1 U/ml). The digested colons were filtered through a 100μm cell strainer and pelleted. Cells were then enriched over an 80/40% Percoll gradient prior to staining or *ex vivo* restimulation. For cytokines production by colonic $CD4^+$ T cells, cells were plated in a round bottom 96-well plate in complete RPMI medium containing PMA (Sigma; final concentration 100ng/mL) and Ionomycin (Sigma; final concentration 10ng/mL) and GolgiPlug (1X - BD Bioscience) and incubated for 4 hours at 37°C 5% CO_2. Cells were then harvested and used for subsequent flow cytometry staining and analysis.

Genomics and sequencing experiments

RNA-seq

Around 100,000 cells were washed once with 1x PBS before resuspending pellet in 350 μL Buffer RLT Plus (QIAGEN) with 1% 2-Mercaptoethanol (Sigma), vortexed briefly, and stored at -80°C. Subsequently, total RNA was isolated using the RNeasy Plus Micro Kit (QIAGEN). RNA integrity numbers were determined using a TapeStation 2200 (Agilent), and all samples used for RNA-seq library preparation had RIN numbers greater than 9. Libraries were prepared using the SMARTer® Stranded Total RNA-seq Kit v2- Pico Input Mammalian kit (Takara). Two technical replicates were generated for each experiment. Libraries were validated for quality and size distribution using a TapeStation 2200 (Agilent). Libraries were paired-end sequenced (38bp+38bp) on a NextSeq 550 (Illumina) or 61bp+61bp on Novaseq 6000 (Illumina).

ATAC-seq

ATAC-seq was performed as previously described with minor modifications.[22] Fifty thousand cells were pelleted at 550 g and washed with 50 μL ice-cold 1x PBS, followed by treatment with 50 μL lysis buffer (10 mM Tris-HCl [pH 7.4], 10 mM NaCl, 3 mM MgCl2, 0.1% IGEPAL CA-630). Nuclei pellets were resuspended in 50 μL transposition reaction containing 2.5 μL Tn5 transposase (FC-121-1030; Illumina). The reaction was incubated in a 37°C heat block for 45 min. Tagmented DNA was purified using a MinElute Reaction Cleanup Kit (QIAGEN) and amplified with varying cycles, depending on the side reaction results. Libraries were purified using a QIAQuick PCR Purification Kit (QIAGEN). Libraries were validated for quality and size distribution using a TapeStation 2200 (Agilent). Libraries were paired-end sequenced (38bp+38bp) on a NextSeq 550 (Illumina) or 61bp+61bp on Novaseq 6000 (Illumina).

Hi-C

Hi-C libraries were generated on 0.5 - $1x10^6$ cells using with Arima-HiC+ kit (Arima Genomics) and Accel-NGS @S Plus DNA Library kit (21024 Swift Biosciences), according to the manufacturer's recommendations. Libraries were validated for quality and size distribution using Qubit dsDNA HS Assay Kit (Invitrogen, cat# Q32851) and TapeStation 2200 (Agilent). Libraries were paired-end sequenced (66bp+66bp) on NovaSeq 6000 (Illumina).

CUT&RUN

CUT&RUN was performed on *in vitro* polarized Th1 cells using CUTANA™ ChIC/CUT&RUN Kit (EpiCypher, Cat#14-1048), using manufacturer's recommendation. Briefly, 4×10^5 live cells were sorted out and nuclei were extracted, washed, and allowed to adsorb

onto activated ConA beads. Cells were then resuspended in recommended buffer, 0.5 mg of antibody was added, mixed well, and allowed to incubate at 4°C overnight on a nutator. Recommended antibodies were used, including anti-H3K27ac (Acetyl-Histone H3 (Lys27) (D5E4) XP® Rabbit mAb, CST, Cat #8173S), anti-ETS-1 (C-20, SantaCruz, Cat# sc-350X) and anti-CTCF (Millipore, Cat# 07-729), along with positive and negative controls. Subsequently, the reactions were washed with cell permeabilization buffer and incubated with pAG-MNase, and the DNA was isolated for the antibody-bound regions. At least two biological replicates were generated for each experiment. Library preparation was carried out using NEBNext Ultra II DNA Library Prep Kit for Illumina (NEB) and were paired-end sequenced (38bp+38bp) on a NextSeq 550 (Illumina) or 61bp+61bp on Novaseq 6000 (Illumina).

Oligopaint FISH probe generation

The OligoMiner pipeline was used to design Oligopaint libraries as performed earlier.[22] 42bp probes were designed to a 50 kbp region at a density of approximately 5 probes per kilobase for the *Ets1* locus using the GRCm38.87 genome.

Oligopaint FISH hybridization

Thymocytes were isolated by dissociating the mouse thymus through a 70 mM filter (Falcon) in RPMI (Corning). Cells were washed with PBS and filtered again. Following this, the cells were diluted to 4 million cells per mL, and 80uL of diluted cells were added to polysine microscope slides (Thermo Scientific, cat#P4981-001) using silicone isolators (Electron Microscopy Sciences, cat #70339-05). Cells adhered to the slides for 1 hour at room temperature inside humidified chambers. Cells were then briefly washed in 1XPBS, fixed in 4% formaldehyde (Fisher Scientific, cat#PI28908) in PBS for 10 min, and then washed in 1XPBS. Slides were stored temporarily in 1xPBS at 4°C or used immediately for DNA FISH. Cells were permeabilized in 0.5% Triton in PBS for 15 min and dehydrated with an ethanol row of 70%, 90%, and 100% ethanol for 2 min each. After allowing the slides to dry for 3-5 minutes, cells were washed in 2XSSCT/50% formamide (0.3M NaCl, 0.03M sodium citrate, 0.1% Tween-20) at room temperature for 5 minutes, 2.5 min at 92°C in 2XSSCT/50% formamide, and 20 min at 60°C in 2XSSCT/50% formamide. For primary probe hybridization, slides were cooled down to room temperature, and cells were immersed in hybridization buffer (10% dextran sulfate, 50% formamide, 4% PVSA, 5.6 mM dNTPs, and 10ug of RNase A) containing 50 pmol of primary Oligopaint probes, covered with a coverslip (Fisher Scientific, cat#12-548-5M), and sealed with no-wrinkle rubber cement (Elmer's). Cells were denatured for 2.5 min at 92°C on top of a heated block, followed by hybridization at 37°C in a humidified chamber for ~16 hrs. Coverslips were then carefully removed using a razor blade, and cells were washed for 15 min in 2XSSCT at 60°C, followed by 10 min wash at room temperature in 2XSSCT shaking at 75 rpm and another 10 min wash at room temperature in 0.2XSSCT. After allowing the slides to air-dry, cells were immersed in secondary hybridization buffer (10% dextran sulfate, 10% formamide, and 4% PVSA) with 2pmol bridges and 10pmol of secondary probes (Alexa-488, Atto-565, and Alexa-647), covered with a coverslip (Fisher Scientific, cat#12-548-5M), and sealed with no-wrinkle rubber cement (Elmer's). Slides were then incubated in the dark in a humidified chamber for 2 hrs at room temperature. Coverslips were then carefully removed using a razor blade, and slides were briefly washed in 2XSSCT at room temperature, followed by a 5 min wash in 2XSSCT at 60°C, a 5 min wash in 2XSSCT with DAPI (0.1 μg/mL), and a 5 min wash in 0.2XSSC.Slide were held in 2XSSC before mounting with Slowfade Gold Antifade Reagent (Invitrogen by Thermo Fisher Scientific, cat#S36936) and sealing with Sally Hansen's "dries instantly top coat".

scRNA- and scATAC-seq library generation

The Chromium Next GEM Single Cell Multiome ATAC + Gene Expression kit (10x Genomics) was used to generate single cell multiome data. Around $1x10^6$ live Th1 cells were sorted, on day 1 and day 6 of *in vitro* Th1 polarization of wildtype and *Ets1*-SE$^{-/-}$ cells. Nuclei isolation was performed based on the manufacturer's instruction (CG000365) with the following modifications. A diluted lysis buffer was made using 10 mM Tris-HCl (pH 7.4), 10 mM NaCl, 3 mM MgCl2, 1% BSA, 1 mM DTT, 1 U/μl RNase inhibitor, and nuclease-free water. Then, 200uL lysis (CG000368) and 400uL diluted lysis buffers were mixed to make the final diluted lysis buffer. Cells were incubated in 100uL final diluted lysis on ice for 5 min. Around 10,000 cells were targeted for recovery per genotype and per time point, and done in replicates. The libraries were generated based on the manufacturer's instruction. All libraries were validated for quality and size distribution using a TapeStation 2200 (Agilent) and quantified using Kapa (Illumina). The scATAC and gene expression libraries were pooled separately and paired-end sequencing (ATAC: Read 1: 50 cycles, i7 Index: 8 cycles, i5 index: 24 cycles, and Read 2: 49 cycle; Gene Expression: Read 1: 28 cycles, i7 Index: 10 cycles, i5 index: 10 cycles, and Read 2: 90 cycle) was performed on the NovaSeq6000 (Illumina).

Genomics Data Analysis

HiChIP data processing and 3D clique analysis

H3K27ac HiChIP measurements in mouse DP T cells were generated in our previous study.[22] Data analysis was performed as previously described: Raw reads for each HiChIP sample were processed with HiC-Pro (version v2.5.0)[65] to obtain putative interactions with default parameters except LIGATION_SITE = GATCGATC and GENOME_FRAGMENT generated for MboI restriction enzyme. Valid pairs (VI), self-circle (SC) and dangling-end (DE) interactions in cis were used as input for significant interaction calling in '.bedpe' format. Mango (version 1.2.0) (Phanstiel et al., 2015) step 4 identified putative significant interaction anchors by MACS peak calling with MACS_qvalue = 0.05 and MACS_shiftsize = 75. Mango step 5 identified significant interactions with default parameters except maxinteractingdist = 2000000 and MHT = found. Two biological repeats for each strain were processed and only significant interactions with PETs >= 2 reproduced in both replicates were used for further analysis. For each library, each significant interaction was normalized to contacts per hundred million, i.e., divided by the number of interactions in the Mango input.bedpe

Please cite this article in press as: Chandra et al., Quantitative control of *Ets1* dosage by a multi-enhancer hub promotes Th1 cell differentiation and protects from allergic inflammation, Immunity (2023), https://doi.org/10.1016/j.immuni.2023.05.004

file and multiplied by 1E8. Mango outputs of two biological replicates where two anchors were within 5kbp were called reproducible interactions in DP T cells.

3D clique analysis

3D clique analysis was performed following the same procedure as reported earlier.[21,22] An undirect graph of regulatory interactions was constructed for reproducible interactions with at least one H3K27ac peak at one anchor. In this graph, each vertex was an enhancer or a promoter and each edge was a significant and reproducible enhancer-enhancer, enhancer-promoter, or promoter-promoter interaction. "3D Cliques" were defined by spectral clustering of the regulatory graph interactions using cluster_louvain function in igraph R package with default parameters. A 3D clique connectivity was defined as the number of edges connecting vertices within the clique. The connectivity of cliques was ranked in ascending order and plotted against the rank. The cutoff for hyperconnected 3D cliques was set to the elbow of the curve and a tangent line at the cutoff was shown. Super-enhancers were defined using H3K27ac ChIP-seq in DP T cells as described earlier.[39] Annotation of noncoding RNA was performed using gencode.vM10.annotation.gtf file. Architectural stripes were defined using Stripenn[26] using Hi-C measurements in DP T cells. Odds ratio analysis was performed to evaluate the significance of enrichment of super-enhancers, ncRNA and architectural stripes.

Hi-C data analysis

Hi-C alignment

We used the ArimaHiC protocol to generate our Hi-C libraries following the manufacturer's recommendations and processed the data with HiC-Pro using parameters "LIGATION_SITE =GAATAATC,GAATACTC,GAATAGTC,GAATATTC,GAATGATC,GACTAATC,GACTACTC,GACTAGTC,GACTATTC,GACTGATC,GAGTAATC,GAGTACTC,GAGTAGTC,GAGTATTC,GAGTGATC,GATCAATC,GATCACTC,GATCAGTC,GATCATTC,GATCGATC,GATTAATC,GATTACTC,GATTAGTC,GATTATTC,GATTGATC" and GENOME_FRAGMENT file was generated using "digest_genome.py -r ^GATC G^AATC G^ATTC G^ACTC G^AGTC". ValidPairs generated by HiC-Pro were further converted to cool and hic files.

Compartment analysis

The principal component analysis (PCA) was performed with 50 kbp resolution for both wild type and Ets1-SE$^{-/-}$ Th1 Hi-C data. To generate the PC1 plot in the Figure S6A, a customized script (cool_compartment.py) utilizing *cooltools* was used.

TAD analysis

TAD coordinates were estimated using two Perl scripts named '*matrix2insulation.pl*' and '*insulation2tads.pl*' from the cworld-Dekker Github page for both wild type and *Ets1*-SE$^{-/-}$ Th1 Hi-C data. The overlap of TAD boundaries was evaluated using the *findOverlaps* function in an R package called GenomicRanges.

Loop analysis

Loops were called using Mustache[66] from both wild type and *Ets1*-SE$^{-/-}$Th1 and Th2 Hi-C with 5kbp resolutions. Loops with FDR < 0.1 were used for further analysis. The scatter plot for loop intensity of wild type and *Ets1*-SE$^{-/-}$ mice was generated, and the loops with intensity higher than |WT/ *Ets1*-SE$^{-/-}$ |>0.5 was highlighted.

Triangle heatmaps

Triangle heatmaps for 3D chromatin conformation data and corresponding tracks were generated using Sushi R package (version 1.28.0)

CUT&RUN data analysis

The FASTQ files of CUT&RUN experiments were aligned to the bam file using BWA (version 0.7.17-r1188). In this process, minor chromosomes such as mitochondrial chromosome or chrY were removed using samtools (version 1.11). Next, duplicated reads were removed using Picard (version 2.26.7) and then the bam files were indexed using samtools. BigWig files were generated using bamCoverage (version 3.3.2) with parameters 'normalizedUsing=CPM, binsize=30, smoothLength=300, p=5, extendReads=200'. For peak calling, macs2 (version 2.1.4) was used with following commands: 'macs2 callpeak -t input_file -c control -g mm -n output_path –nomodel -f BAMPE -B –keep-dup all –broad –broad-cutoff 0.25 -q 0.25'. For the background (control), the bam file of IgG CUT&RUN data was used. CUT&RUN peaks from two conditions and both replicates were merged and the number of fragments in each peak were counted with bedtools. The count data of each peak was then fed to DESeq2 for differential analysis.

Integration of CUT&RUN data with 3D loop analysis

Loop classification

The loops called from the wild type Th1 Hi-C with 5kb resolution were classified based on the occupancy of CTCF and/or ETS1. First, the CTCF and ETS1 peaks from replicates were combined, respectively. Next, both ends of each loop (loop anchors) were extended by ±5 kbp and then the occupancy of CTCF or ETS1 peaks within loop anchors was examined using the R package named GenomicRanges.

DESeq2 analysis and pileup plot

To identify CTCF and ETS1 peaks that were lost or gained in a coordinated manner in *Ets1*-SE$^{-/-}$ Th1 cells, DESeq2 was performed by (1) combining CTCF and ETS1 peaks across all replicates, (2) counting reads across this union of peaks, and (3) comparing wildtype and *Ets1*-SE$^{-/-}$ Th1 cells samples regardless of the protein occupancy. As a result, 988 and 364 co-bound CTCF-ETS1 peaks were detected to be co-lost and co-gained, respectively (|log2 fold change| > 1 and p-value<0.05). 1D heatmaps using deeptools or pileup plots for 3D interactions using coolpuppy examined the 1D and 3D features of these peak sets. For coolpup.py, a parameter –pad=50 was used. Local pileup analysis at different sets of peaks was done with coolpup.py 63 using parameters "–pad 250–local". The

average interaction of the upright corner of pileup plots is quantified with custom python script, by parsing the results from coolpup.py. Interactions between regions in bedfiles were done with parameters "–mindist 200000 –maxdist 2000000". Pileup of loops was also plot with coolpup.py. To do multiple pileup analysis parallelly, we used GNU parallel to run the shell script.

Deeptools analysis of CUT&RUN and ATAC-seq data

The differentially gained or lost sites in Naive CD4$^+$ T, Th1 and Th2 cells were obtained using DESeq2 (|log2 fold change| > 1 and adjusted p-value<0.05) and then combined using bedtools sort and merge function. Next, deeptools plot was generated with computeMatrix function using following parameters: reference-point –referencePoint center -a 2000 -b 2000. The heatmap was generated with the 'plotHeatmap' function with the following parameters: '–heatmapHeight 15 –averageTypeSummaryPlot median –colorMap Greys'. In comparison of Naive CD4 T and Th1 cells, we performed DESeq2 for Naive CD4 T and Th1 cells (*Ets1*-SE+/+). Then, Naive CD4 T-specific ($\log_2$ fold change > 1 and adjusted P-value < 0.05), Th1-specific ($\log_2$ fold change < -1 and adjusted P-value < 0.05) and non-significant (adjusted P-value > 0.05) peaks were obtained and fed to computeMatrix/plotHeatmap function.

RNA-seq data analysis

The FASTQ files of RNA-seq experiments were aligned and further counted using STAR 2.7.7a with parameters '–outSAMtype BAM SortedByCoordinate –outWigType wiggle read1_5p –outWigStrand Stranded –outWigNorm RPM–quantMode GeneCounts'. Next, DESeq2 was performed to identify differentially expressed genes (|log2 fold change|>1 and adjusted p-value < 0.05).

ATAC-seq data analysis

The alignment process of ATAC-seq data is identical to that of CUT&RUN data except MACS2 parameters which is as follows: 'macs2 callpeak -t input_file -g mm -n output_path –nomodel -f BAM -B –keep-dup all –broad –broad-cutoff 0.1 -q 0.1'. ATAC-seq peaks from two conditions and both replicates were merged and the number of fragments in each peak were counted with bedtools. The count data of each peak was then fed to DESeq2 for differential analysis.

scRNA- and scATAC-seq data preprocessing and quality control

The cellranger-arc mkfastq from Cell Ranger ARC pipeline (version 2.0.0) was used to demultiplex samples. Demultiplexed scRNA- and scATAC-seq fastq files were inputted into the cellranger-arc count pipeline from 10x Genomics to generate barcoded count matrices of gene expression and ATAC data. cellranger-arc aggr was used to aggregate samples across all conditions. For the aggregate of all samples, count matrices were loaded in Seurat pipeline and selected for barcodes that appeared in both the scRNA-seq and scATAC-seq datasets. scRNA-seq data from nuclei remaining after quality control filtering were analyzed using Seurat (version 4.3). Gene expression counts were normalized using the SCT function. Graph-based clustering was then performed on the data using the top 20 principal components at a resolution of 0.5. Cluster identities were manually annotated based on the expression of genes from published scRNA-seq studies of T cell differentiation. Marker genes for each cluster were additionally identified using the FindAllMarkers function with a minimum fraction of 0.5 and a $\log_2$ fold change of 1. Clusters expressing low RNA count were removed from further analysis. scATAC-seq data were analyzed using Signac (V 1.9.0) based on barcoded cell type identities from scRNA-seq. Chromatin accessibility peaks on chromosomes 1-22 and X and outside of blacklist regions were then called using the MACS2 with scATAC peaks for all cells.

GSEA and Gene Ontology analysis

Pre-ranked Gene Set Enrichment Analysis (GSEA) was used for enrichment analyses. Gene-sets were provided by DESeq2 for down-regulated and upregulated genes in *Ets1*-SE$^{-/-}$ compared with wildtype Th1 cells. Pre-ranked genes based on DESeq analysis of across different conditions were used. Metascape using ImmuneSigDB was used for gene-ontology analysis.

ImmGen gene expression data processing

Gene Skyline feature for RNA-seq data provided by ImmGen was used to profile Ets1 and Fli1 expression levels across various cell types.

Motif analysis

To find the conserved motifs from the lost or gained ATAC-seq/Hi-C peaks(=loops) in *Ets1*-SE$^{-/-}$ mice, a function named 'findMotifsGenome.pl' in Homer program (version 4.11) was utilized. For ATAC-seq data of naive CD4 T cells, gained and lost peaks in *Ets1*-SE$^{-/-}$ mice were determined by DESeq2 results such that |log2 fold change| > 1 and adjusted P-value < 0.05. Here, the peaks that were not significantly changed (adjusted P-value>0.8) were used as background. The loops gained and lost in Ets1-SE were searched from Hi-C data of Th1 cells. Here, gained and lost loops were defined as those |fold change|>0.5, and the loops showing minute changes (|fold change| < 0.1) were considered as background. These loop coordinates were then fed to 'bedtools intersect (version 2.30.0)' to obtain the coordinates overlapping with CUT&RUN peaks of ETS1.The output consists of (1) consensus motifs (known motifs) and (2) de novo motifs conserved in the input sequences (homer motifs). Here, we reported the latter one.

Oligopaint FISH imaging and analysis

Imaging was carried out on a Bruker Vutara VXL in the Widefield imaging modality, which has an imaging field-of-view (FOV) of 200 μm x 200 μm. The VXL has a 60X silicon oil immersion objective with a 1.3 numerical aperture (NA). Z-stack size was maximum 20 μm with a Z-step size of 150 nm. Analysis was carried out on the raw images in a semi-automated manner on a cell-by-cell basis as describe in Raj et al. 2008 (https://github.com/arjunrajlaboratory/rajlabimagetools). Briefly, the DAPI signal was used for manual nuclei segmentation of DP T cells. The exact numbers of nuclei analyzed per genotype are as follows: 561 nuclei for wildtype and 727 nuclei for the cells from *Ets1*-SE$^{-/-}$. One mouse per genotype was used. Spots for each of the 3 channels (Alexa-488, Atto-565, and Alexa-647) were individually detected using a linear filter approximately conforming to a Laplacian convolved with a

Gaussian. For each spot, the brightest z slice was used as the z coordinate. Centroid positions for each spot in xy were found by fitting a Gaussian. X, Y, and Z coordinates were extracted, and pairwise Euclidean distances between nearest neighbors were calculated. The spatial distance of two probes in each cell were determined by taking a minimum from all pair-wise distances of corresponding probes. The Kolmogorov-Smirnov test was used to compare differences in the cumulative distributions, and the Mann-Whitney test was used to compare differences in the medians. In addition, the proportion of cells having probe distance less than threshold was examined for 3D clique dynamics analysis.

Representative Image processing

Imaging was carried out on a Leica Multiphoton Confocal using a 63X oil immersion objective with a 2.0 zoom factor, a pixel size of 58.77 nm x 58.77 nm, and Z-stack size of 15 μm with a Z-step size of 300 nm. Z-stacks were maximally projected. Each cell, allele, and locus for each strain were individually processed using ImageJ via adjusting the brightness/contrast/minimum/maximum, as well as smoothing.

Ets1$^{+/-}$ mice data analysis

Virtual 4C analysis

The Virtual 4C analysis evaluates the DNA interaction that takes place between a genomic anchor and the loci located in its proximity. Here, the direct downstream of Gm27162 was set as an anchor, and its normalized contact frequencies (VC_SQRT) with the *Ets1-Fli1* region (chr9:32325001-33205000) were measured using Hi-C data of *Ets1*-SE$^{-/-}$, and *Ets1*$^{fl/+}$*Cd4*^{cre} Th1 cells and their wildtype counterparts. Instead of the commonly used line plots, virtual 4C plot here is represented by a heatmap to effectively compare the contact frequencies from four datasets.

Loop analysis

From the Hi-C data of *Ets1*-SE$^{-/-}$ naïve CD4+ T cells, *Ets1*-SE$^{-/-}$ Th1 cells, *Ets1*$^{fl/+}$*Cd4*^{cre} Th1 cells and their wildtype counterparts, 11031, 13164, 17790, 15642, 18077 and 17818 long-range interactions were detected using Mustache (version 1.2.7, FDR<0.1). The loops from six datasets were then merged into 67119 loops using *sort* and *uniq* command in Linux to collect as many loops as possible for testing. Next, by utilizing the balancing in the python cooler package, the normalized contact frequencies were calculated for *Ets1*-SE$^{-/-}$ and *Ets1*$^{fl/+}$*Cd4*^{cre} Th1 cells and their wildtype counterparts. Upon calculating the fold change, we found 5,787 loops that exhibited simultaneous alterations with Ets1 dose reduction ($|\log_2 FC|>0.25$).

ChIP-Atlas

ChIP-Atlas is a comprehensive database that collects public ChIP-seq, DNase-seq, ATAC-seq and Bisulfite-seq data. It provides an integrative analysis such as peak browser, TF target gene search, colocalization and enrichment analysis. In this study, peak browser was utilized to search for the transcription factors bound on Gm27162 locus in Th1 cells. Experiment type, cell type class, threshold for significance and cell type were set as ChIP:TFs and others, blood, 50 and Th1 cells, respectively. The bed file was further processed with *awk* to include TFs bound on Gm27162 region.

Allergy-associated SNPs enrichment

A list of 58 SNPs within Ets1-Fli1 region was manually collected. The orthologous human coordinate of Gm27162 (chr11:128303536-128330986) included 9 SNPs in total. Among them, four were related to allergy/asthma. *P*-value and odds ratio were estimated by Fisher exact test using *fisher.test* function in R stats package.

Statistical analysis

For all experiments, the difference between two groups was calculated using unpaired t-test (Mann and Whitney) Prism 10 GraphPad Software. ANOVA and Bonferroni test were used for multiple comparisons (ns = not significant, * = $p \leq 0.05$, ** = $p \leq 0.01$, *** = $p \leq 0.0005$, **** = $p \leq 0.0001$). The Mann and Whitney unpaired t-test was used for comparisons of two conditions within one group. One-way ANOVA was used to compare more than two conditions for one group. The Two-way ANOVA was used to compare two conditions across multiple groups. All graphs show the mean and the standard error of the mean (SEM). One- and Two-way ANOVA were corrected for multiple comparison using Bonferroni correction.